

SFMP: Fine-Grained, Hardware-Friendly and Search-Free Mixed-Precision Quantization for Large Language Models

Xin Nie¹ Haicheng Zhang¹ Liang Dong¹ Beining Feng¹ Jinhong Weng¹ Guiling Sun¹

Abstract

Mixed-precision quantization is a promising approach for compressing large language models under tight memory budgets. However, existing mixed-precision methods typically suffer from one of two limitations: they either rely on expensive discrete optimization to determine precision allocation, or introduce hardware inefficiencies due to irregular memory layouts. We propose **SFMP**, a search-free and hardware-friendly mixed-precision quantization framework for large language models. The framework is built upon four novel ideas: 1) *Fractional bit-width*, which extends integer bit-width for weight matrix to fractional value and transforms discrete precision allocation as a continuous problem; 2) *Block-wise mixed-precision*, enabling fine-grained precision within weight matrices while remaining hardware-friendly; 3) *Row-column weight reordering*, which aggregates salient weights via row and column reordering, incurring only a small activation reordering overhead during inference; 4) *Unified GEMM kernel*, which supports mixed-precision GEMM at arbitrary average bit-width. Extensive experiments demonstrate that SFMP outperforms state-of-the-art layer-wise mixed-precision methods under the same memory constraints, while significantly reducing quantization cost and improving inference efficiency. Code is available at <https://github.com/Nknixin/SFMP>

1. Introduction

Weight quantization is an efficient approach to compressing large language models (LLMs). It requires no modifications to the model architecture and directly maps high-precision continuous weights to a discrete space, reducing the average bits of model parameters, which enables deployment of

¹College of Electronic Information and Optical Engineering, Nankai University, Tian Jin, China. Correspondence to: Guiling Sun <sungl@nankai.edu.cn>.

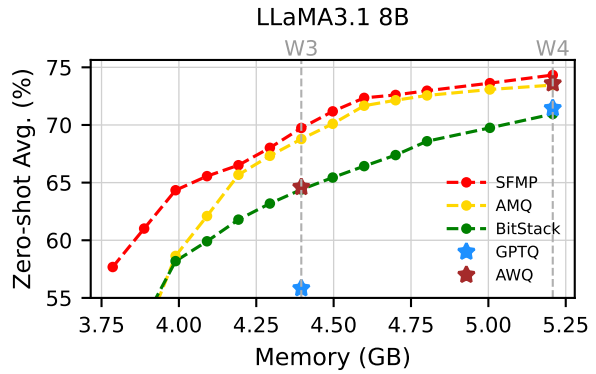


Figure 1. Trade-off between memory usage and average zero-shot accuracy on ARC-Easy, ARC-Challenge, PIQA, HellaSwag, WinoGrande, and BoolQ.

LLMs in memory-constrained edge scenarios (Zhang et al., 2024; Hosseinzadeh & Khamroush, 2025; Husom et al., 2025). Existing methods (Frantar et al., 2023; Xiao et al., 2023; Lin et al., 2024; Kim et al., 2024; Liu et al., 2025b) achieve near-lossless compression at 8-bit precision and only incur 1–3% accuracy loss at 4-bit.

For ultra-large models, such as LLaMA3.1-70B, assigning a uniform integer bit-width to all linear layers limits the choices of model size and cannot adapt to diverse memory budgets. To address this limitation, layer-wise mixed-precision quantization (Lee et al., 2025; Cheng et al., 2025; Liu et al., 2025a; Dong et al., 2020) assigns different integer bit-widths to each linear layer, enabling flexible compression under given memory constraints. However, from an optimization perspective, layer-wise mixed-precision quantization constitutes a constrained integer programming problem (ILP), which is known to be NP-hard (Hochba, 1997). For example, for LLaMA3.1-70B (560 weight matrices) with candidate bit-widths {2, 3, 4}, the search space is 3^{560} . Existing methods typically transform the problem to fit off-the-shelf ILP solvers (Bellman, 1966; Wolsey, 2020) or heuristic algorithms (Deb et al., 2002; Kirkpatrick et al., 1983) to obtain a relatively good solution in a short time. Even so, state-of-the-art layer-wise mixed-precision methods AMQ (Lee et al., 2025) still require 44 hours to search for the bit allocation of LLaMA3.1-70B. This raises a question: **“Under a given memory budget, can we design a strategy to obtain a near-optimal bit allocation without**

any search or solver-based optimization?”

Beyond layer-wise mixed-precision quantization, many methods introduce finer-grained strategies, such as channel-wise (Zihan et al., 2025; Wang et al., 2024), group-wise (Huang et al., 2025; Hooper et al., 2025), or even element-wise schemes (Kim et al., 2024; Zhao & Yuan, 2025; Li et al., 2023) in a weight matrix. Although such strategies can further improve model accuracy, they induce irregular memory access patterns and incur substantial overhead in weight packing and unpacking, which significantly degrades inference performance. Some approaches (Kim et al., 2024; Zihan et al., 2025) attempt to mitigate this inference speed degradation with custom compute kernels (Li et al., 2024; Qin et al., 2020; Liu et al., 2025c). However, the resulting speedup is limited. Additionally, combining these fine-grained schemes with layer-wise mixed-precision further complicates the discrete optimization problem. This raises another important question: “**Can we design a quantization format that achieves fine-grained mixed-precision while remaining hardware-friendly?**”

In this paper, to address these limitations, we propose **SFMP**, a **Search-free Mixed-precision** framework. SFMP eliminates the need to solve complex integer programming problems under memory constraints, reducing the time required for compressing LLMs. Moreover, SFMP introduces a fine-grained yet hardware-friendly quantization format that organizes memory and executes matrix computations in a unified manner. SFMP is built upon four key ideas: 1) **Fractional bit-width**: we extend integer bit-width for weight matrix to fractional value, transforming mixed-precision quantization from a discrete, combinatorial optimization problem into a continuous problem; 2) **Block-wise mixed-precision**: a format achieves fine-grained mixed-precision while remaining hardware-friendly; 3) **Row-column weight reordering**: weights are reordered along rows and columns to aggregate salient weights and align with the block-wise format, incurring only a small activation reordering overhead during inference; 4) **Unified GEMM kernel**: for weight matrices with arbitrary average bit-width, we propose a unified kernel for memory layout and mixed-precision GEMM execution. As shown in Fig. 1, our method achieves superior quantized model performance compared to state-of-the-art layer-wise mixed-precision method (Lee et al., 2025) under the same memory footprint.

2. Related Works

Salience-Aware Mixed-Precision Quantization. Weight salience is widely used to guide mixed-precision quantization. SqueezeLLM (Kim et al., 2024) computes the global Fisher Information Matrix (Ly et al., 2017) and retains a small set of salient weights in high precision. BiLLM

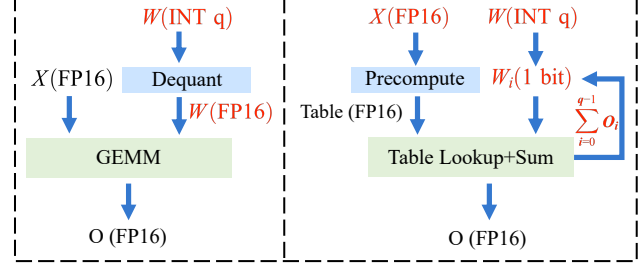


Figure 2. Comparison of two GEMM computation paradigms: Left) dequant-based GEMM; Right) one-bit LUT-based GEMM.

(Huang et al., 2024) observes that salience often concentrates along specific rows or columns and reduces quantization error through column-wise partitioning. Similarly, Slim-LLM (Huang et al., 2025) exploits row-wise salience by introducing group-wise mixed-precision quantization, achieving improved accuracy over fixed-precision schemes under the same average bit-width.

One-bit LUT-Based GEMM. Some prior works (Wei et al., 2025; Park et al., 2025b; 2024; You et al., 2024; Ganji et al., 2023; Park et al., 2025a) introduce a dequantization-free compute paradigm for FP-INT GEMM. As shown in Fig. 2, a q -bit quantized weight matrix is decomposed into q one-bit matrices. For an activation vector of group size g , the dot products between the activation and all 2^g possible binary patterns are precomputed and stored in a lookup table (LUT). Consequently, the GEMV operation between the activation vector and the one-bit weight matrix can be replaced by LUT accesses and accumulation. This paradigm eliminates the overhead of weight unpacking at runtime, particularly for ultra low-bit quantization. Moreover, it provides a unified computation kernel: The GEMM computation between activation and a weight matrix of arbitrary integer bit-width can be expressed as a linear combination of one-bit GEMMs. Owing to its LUT-dominated execution, this paradigm has been demonstrated to be energy-efficient (Jeon et al., 2020; Cicek et al., 2022; Kim et al., 2025), making it especially suitable for edge devices. A detailed description of the computation flow is provided in Appendix B.

3. Motivation

High Cost of Layer-Wise Bit Allocation. As shown in Fig. 3, layer-wise mixed-precision quantization (Tang et al., 2022; Ranjan & Savakis, 2024; Zhao et al., 2024; Ranjan & Savakis, 2025) requires solving a discrete optimization problem, leading to an exponentially large search space as the number of layers grows. Although heuristic methods can reduce the search complexity, obtaining a satisfactory configuration remains costly in practice. For example, AMQ (Lee et al., 2025) requires around 44 hours to search mixed-precision configuration for LLaMA3.1-70B. This motivates the development of search-free bit allocation strategies that scale efficiently to large models.

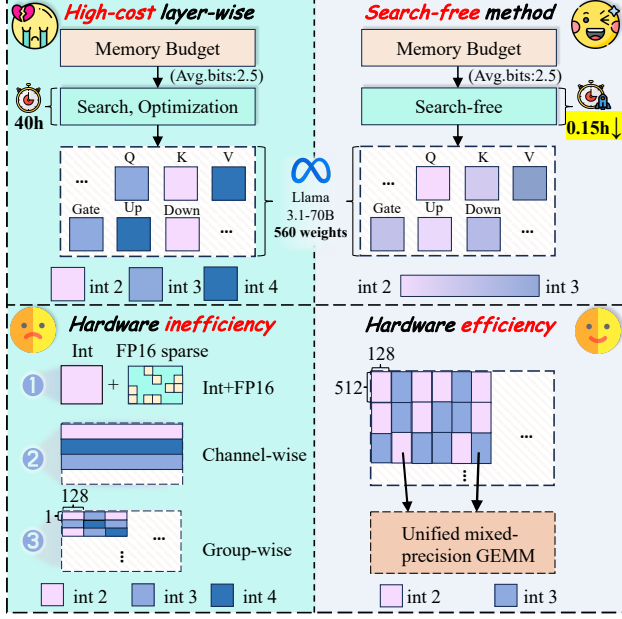


Figure 3. Motivation of SFMP.

Hardware Inefficiency of Element-, Group-, and Channel-Wise Quantization. Despite their accuracy benefits, fine-grained mixed-precision schemes are often misaligned with efficient hardware execution. As illustrated in Fig. 3, element-wise methods store sparse high-precision weights, introducing additional sparse storage. Channel-wise or group-wise methods partially improves regularity, yet still incur irregular memory access patterns. These characteristics limit the inference throughput in practical deployment. For example, our empirical study in Fig. 12 shows that the group-wise mixed-precision method SliM-LLM (Huang et al., 2025) suffers 30–50% lower inference throughput than GPTQ (Frantar et al., 2023) at the same average bit.

Structured Clustering of Salient Weights. Several prior studies (Lin et al., 2024; Huang et al., 2024; 2025) have shown that the distribution of weight salience exhibits structured patterns, typically aligned along rows or columns of the weight matrix. This behavior is commonly attributed to the convergence properties of the multi-head self-attention mechanism. However, as shown in Fig. 13, the weight salience is often scattered within rows or columns rather than forming compact blocks. This observation motivates our reordering strategy, which aligns the salient weight with hardware-friendly memory organization.

4. SFMP

4.1. Preliminaries

Global Salience of Weights. Weights in large language models exhibit heterogeneous salience to the final model loss. We estimate the global salience of weights by analyzing their impact on the model’s output loss.

Assuming the model has converged, the loss variation $\Delta\mathcal{L}$ induced by a perturbation from W to W' can be approximated by a second-order expansion:

$$\Delta\mathcal{L} \approx (W - W')^\top H(W - W'), \quad (1)$$

where H denotes the Hessian of the global loss with respect to weights. Since computing the full Hessian is intractable for large-scale models, we approximate it using the Fisher Information Matrix (Ly et al., 2017),

$$H \approx \mathcal{F} = \mathbb{E}[gg^\top], \quad (2)$$

where g denotes the gradient of the loss with respect to the weights, and the expectation is taken over a small calibration dataset. Following prior work (Kim et al., 2024), we adopt a diagonal approximation by ignoring cross-weight interactions. Therefore, the Fisher diagonal values can serve as salience scores, reflecting the importance of individual weights to the final output. Detailed derivations are provided in Appendix C.

Notation. For the l -th weight matrix $W_l \in \mathbb{R}^{m \times n}$, we denote its corresponding global salience matrix by $S_l \in \mathbb{R}^{m \times n}$. Each entry $S_{l,i,j}$ represents the salience of the weight element $W_{l,i,j}$, as estimated by the diagonal values of the global Fisher Information Matrix.

4.2. Fractional Bit-Width for Weight Matrix

Let the set of candidate integer bit-widths be

$$\mathcal{B} = \{b_1, b_2, \dots, b_q\}, \quad b_i \in \mathbb{Z}_{>0}. \quad (3)$$

In the layer-wise mixed-precision method, all weights in a weight matrix have the same quantization bit-width. we refine the minimum unit of bit allocation to individual weight elements. Then, the mixed-precision quantization problem can be formulated as follows: given a target average bit $b \in \mathbb{R}_{>0}$, find a set of coefficients $\{\alpha_1, \alpha_2, \dots, \alpha_q\}$ such that

$$\sum_{i=1}^q \alpha_i = 1 \quad \text{and} \quad \sum_{i=1}^q \alpha_i b_i = b, \quad (4)$$

under which an optimal element-wise quantization bit-width is assigned to each weight. In fact, solving this optimization problem can obtain an optimal quantized model, as element-wise allocation provides finer granularity than layer-wise methods. However, this optimization problem is highly challenging due to the massive number of parameters in large language models. As the model size and the number of candidate integer bit-widths increase, the problem complexity grows exponentially. To make the problem tractable, we restrict the element-wise bit-width choices to a small set of candidate values.

The empirical study from CMPQ (Zihan et al., 2025) provides a insight: “at an average bit-width of 3, 4-bit weights are often insufficient to compensate the errors introduced

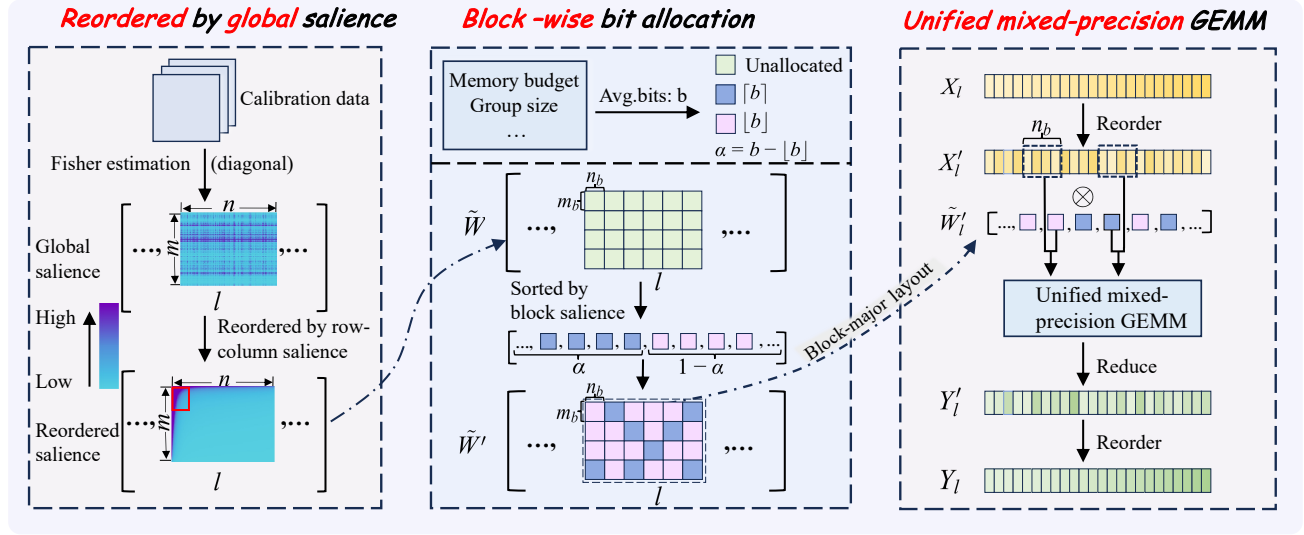


Figure 4. Pipeline of SFMP.

by 2-bit weights”. Inspired by this observation, we limit the candidate bit-width set to two values, with the difference between them not exceeding 1. Therefore, for a given average bit b , the candidate quantization bit-widths are uniquely determined as:

$$\mathcal{B} = \{\lfloor b \rfloor, \lceil b \rceil\}, \quad (5)$$

where $\lfloor \cdot \rfloor$ denotes the floor function and $\lceil \cdot \rceil$ denotes the ceiling function. The bit allocation problem now simplifies to a binary optimization problem under the constraints:

$$\alpha_1 + \alpha_2 = 1, \quad \alpha_1 \lfloor b \rfloor + \alpha_2 \lceil b \rceil = b. \quad (6)$$

Considering the global salience of weights, a natural and effective allocation strategy is to assign higher bit-widths to more salient weights. Specifically, let $\alpha = b - \lfloor b \rfloor$ represent the fractional part of b . The bit-width allocation strategy for weight $\{W_l\}_{l=1}^L$ is:

$$\text{bit}(W_{l,i,j}) = \begin{cases} \lceil b \rceil, & S_{l,i,j} \geq \tau_\alpha, \\ \lfloor b \rfloor, & \text{otherwise,} \end{cases} \quad (7)$$

where τ_α denotes the α -quantile of S . Notably, once the average bits b is specified, this strategy directly yields the bit allocation without solving any optimization problem. Under this scheme, the average bit-width of each weight matrix is no longer an integer but a fractional value.

4.3. Block-Wise Mixed-Precision

However, although the element-wise bit allocation strategy is theoretically accurate and simple to implement, it is not hardware-friendly. This is because weights assigned the same quantization bit-width in a weight matrix are distributed in a highly irregular spatial pattern, which makes structured quantization difficult.

To balance quantization performance and hardware efficiency, we adopt a coarser but structured block-wise bit

allocation strategy. That means the bit-widths are assigned at the block level rather than to individual weights. Specifically, each weight matrix W_l is partitioned into a set of non-overlapping two-dimensional blocks of size $m_b \times n_b$, denoted as

$$\{B_{l,1}, B_{l,2}, \dots, B_{l,K_l}\}, \quad B_{l,k} \in \mathbb{R}^{m_b \times n_b}. \quad (8)$$

We define the global salience of a block as the sum of the global salience values of all weights contained within it. Formally, the salience of the k -th block in the l -th weight matrix is given by

$$\text{Sal}(B_{l,k}) = \sum_{(i,j) \in B_{l,k}} S_{l,i,j}. \quad (9)$$

Based on the block-level salience, we treat each block as the minimum decision unit for bit allocation. Consistent with the element-wise strategy, we select a threshold $\tau_\alpha = \text{Quantile}_\alpha(\{\text{Sal}(B_{l,k})\}_{l=1, k=1}^{L, K_l})$ and define the block-wise bit allocation as:

$$\text{bit}(B_{l,k}) = \begin{cases} \lceil b \rceil, & \text{if } \text{Sal}(B_{l,k}) \geq \tau_\alpha, \\ \lfloor b \rfloor, & \text{otherwise.} \end{cases} \quad (10)$$

This block-wise strategy identifies high-salience regions in a more structured manner, yielding regular and hardware-friendly bit patterns. In practice, the block dimensions (m_b, n_b) are determined by balancing fine-grained granularity and hardware characteristics. For example, on GPUs, we adopt block sizes such as (256, 128) or (512, 128) to match common GEMM tiling strategies and warp-level parallelism in CUDA.

4.4. Row-Column Weight Reordering

As mentioned in Section 3, the spatial distribution of weight salience is primarily structured along rows or columns,

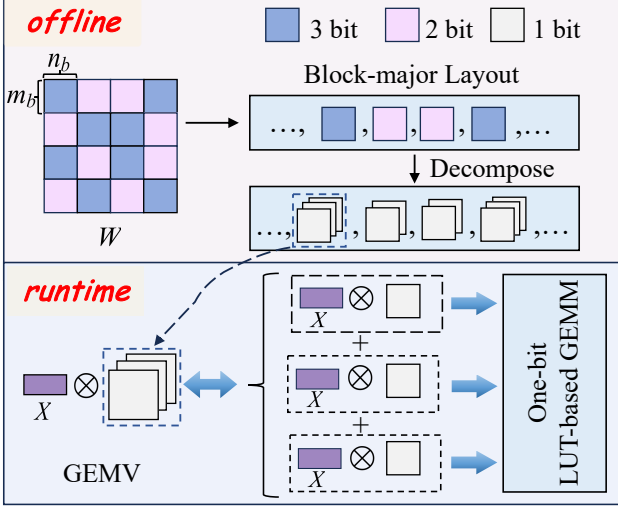


Figure 5. An example of unified mixed-precision GEMM.

rather than forming spatially contiguous block-level clusters. Consequently, block-wise bit allocation is spatially misaligned with the salience patterns. Therefore, prior to block-wise bit allocation, we reorder the weight matrix based on row and column salience to achieve block-level aggregation of salient weights.

Given the salience matrix $S_l \in \mathbb{R}^{m \times n}$, we compute row- and column-wise salience by summation,

$$s_{l,\text{row}} = S_l \mathbf{1}, \quad s_{l,\text{col}} = S_l^\top \mathbf{1}, \quad (11)$$

where $\mathbf{1}$ denotes the all-ones vector. Row and column permutations are then obtained by sorting the salience vectors in descending order,

$$p_{l,\text{row}} = \text{argsort}(s_{l,\text{row}}), \quad p_{l,\text{col}} = \text{argsort}(s_{l,\text{col}}). \quad (12)$$

Let $P_{l,\text{row}}$ and $P_{l,\text{col}}$ denote the corresponding permutation matrices. The reordered weight matrix is given by

$$\tilde{W}_l = P_{l,\text{row}} W_l P_{l,\text{col}}. \quad (13)$$

As shown in Fig. 4, the reordering strategy spatially aggregate high-salience weights, improving the alignment between weight salience and block-wise bit allocation. Notably, the reordering is performed offline and incurs no runtime overhead. During inference, As shown in Eq. 14, the reordering can be equivalently applied to the activation X_l , whose cost is negligible compared to the GEMM operation.

$$X_l W_l^T = X_l (P_{l,\text{col}}^T)^{-1} \tilde{W}_l^T (P_{l,\text{row}}^T)^{-1}. \quad (14)$$

4.5. Unified Mixed-Precision GEMM Kernel

For our proposed block-wise mixed-precision format, adopting dequant-based operators introduces two major challenges: 1) conventional row-major or column-major storage layouts complicate weight packing and unpacking, as

the block structure is not explicitly represented in memory. 2) mixed-precision formats require additional control-flow branching and multiple kernel variants in compute kernels (e.g., CUDA kernels), increasing implementation complexity.

As shown in Fig. 5, to address challenge 1), we propose a block-major representation, where the quantized weight matrix is partitioned into blocks according to the (m_b, n_b) selected in Eq. 8 and organized in a block-major layout, enabling contiguous memory access within each block. To address challenge 2), we employ a unified GEMM kernel that processes all blocks regardless of their bit-widths. Specifically, each block is decomposed into one-bit components and computed via one-bit LUT-based GEMM, thereby eliminating explicit weight dequantization and precision-specific execution paths (see Appendix G for detailed CUDA implementation).

4.6. Pipeline of SFMP

Fig. 4 shows the pipeline of SFMP. First, SFMP reorders weight matrices by global salience and partitions them into fixed-size blocks. Second, based on the memory budget and other configurations, SFMP computes the average bits b and selects two candidate precisions $\lfloor b \rfloor$ and $\lceil b \rceil$. Then, SFMP assigns $\lceil b \rceil$ to a fraction $\alpha = b - \lfloor b \rfloor$ of the most salient blocks, with the rest using $\lfloor b \rfloor$. Finally, we organize weights in a block-major layout and convert each weight block into the one-bit format, enabling unified execution using the one-bit LUT-based GEMM. The entire pipeline is parameter-free and requires no search or iterative optimization.

5. Experiments

We evaluate our method on several state-of-the-art pre-trained models, including LLaMA3.1 8B and 70B (Dubey et al., 2024), Qwen3 8B, 14B and 32B (Yang et al., 2025). Weight salience is estimated by computing the Fisher Information Matrix following SqueezeLLM (Kim et al., 2024), using 1k samples from C4 (Raffel et al., 2020). The block shape (m_b, n_b) is (512, groupsize), where group quantization is applied along the n_b dimension within each block. To ensure fair comparison, following AMQ (Lee et al., 2025), we avoid introducing complex tricks and just adopt AWQ (Lin et al., 2024) as our quantization method. We compare our method against fixed-precision methods such as GPTQ and AWQ, group-wise mixed-precision method SLIM-LLM (Huang et al., 2025), any-size methods such as BitStack (Wang et al., 2025) and AMQ. Our method is orthogonal to most quantization tricks, in Appendix I, we further combine our approach with Quantization-Aware Training (QAT) method (Chen et al., 2024). All experiments are conducted on A100-80GB GPU.

We evaluate our method from multiple perspectives. For language modeling, we report perplexity on C4 and WikiText2

(Merity et al., 2017). For zero-shot evaluation, we use the LM Evaluation Harness (Gao et al., 2021) to evaluate six tasks, including ARC-Challenge, ARC-Easy (Clark et al., 2018), PIQA (Bisk et al., 2020), HellaSwag (Zellers et al., 2019), BoolQ (Clark et al., 2019), and WinoGrande (Sakaguchi et al., 2021). We further evaluate 5-shot performance on MMLU (Hendrycks et al., 2020) and GSM8K (Cobbe et al., 2021). For inference performance, considering edge deployment scenarios, we report both kernel-level latency and end-to-end inference speed (tokens / s) when generating 128 tokens with batch size 1.

5.1. Main Results

SFMP vs. Any-Size Methods. Table 1 reports the model perplexity and zero-shot task accuracy under different memory budgets for models quantized with SFMP, AMQ, and BitStack. We report results under different **BPW** (bits per weight) settings. Across multiple model scales, SFMP consistently outperforms AMQ. The advantage of SFMP becomes more pronounced at extremely low precision (e.g., BPW=2.5), where it achieves the best average zero-shot accuracy among all methods. At BPW=3.5, SFMP retains 98.90% of the average zero-shot performance of the FP16 LLaMA3.1-70B model. Moreover, Table 2 shows that on the 5-shot MMLU and GSM8K benchmarks, SFMP consistently outperforms AMQ across all model sizes. These results demonstrate that SFMP remains robust on challenging tasks and show that our strategy is more stable and effective than layer-wise mixed-precision methods, even without any search or optimization.

SFMP vs. Fixed-Precision Methods. We compare SFMP with GPTQ, AWQ and SliM-LLM, which apply a uniform bit-width across all weight matrices. Table 3 reports perplexity and average zero-shot accuracy on the BPW ranging from 2.25 to 4. Across all settings, SFMP consistently outperforms fixed-precision methods. For both LLaMA3.1 8B and LLaMA3.1 70B, GPTQ and AWQ exhibit a sharp performance degradation at BPW=2.25. In contrast, by setting the group size to 256, SFMP enables 12.5% of the weights to be quantized at 3-bit, which substantially mitigates this degradation and leads to significantly improved performance. This reveals an important trend: under a fixed memory budget, moderately increasing the group size thereby allocates more memory budget to weight bit-width rather than scales and zero-points, leading to improved model performance. We provide a detailed analysis in Appendix H.1. Moreover, SFMP consistently outperforms the group-wise mixed-precision method SliM-LLM and provides greater flexibility in precision allocation, as SliM-LLM enforces fixed average bit-width across all weight matrices.

Inference Performance. We evaluate the inference performance of SFMP across a wide range of hardware platforms. As shown in Fig. 6, fixed-precision uniform quan-

Table 1. Evaluation of Llama 3.1 8B/70B models compressed by SFMP, BitStack and AMQ at the BPW of 2.5, 3.0, 3.5 and 4.0, using a groupsize of 128, showing WikiText-2 and C4 dataset perplexity (PPL) alongside zero-shot tasks average accuracy. **BPW** denotes “bits per weight”. Quantization scales and zero-points are stored in FP16. Detailed zero-shot accuracy is provided in Table 11.

Model	Mem. (MB)	BPW	Method	Wiki(↓)	C4(↓)	Avg.(↑)
8B	15,317	16	FP16	6.15	8.89	75.01
	4,085	2.5	BitStack	23.28	38.23	58.19
			AMQ	17.85	24.01	58.65
			SFMP	14.49	18.81	64.34
	4,501	3.0	BitStack	12.55	20.47	64.40
			AMQ	9.38	13.05	68.78
			SFMP	9.51	13.13	69.74
70B	4,917	3.5	BitStack	9.47	15.29	68.59
			AMQ	7.39	10.54	72.56
			SFMP	7.19	10.28	72.97
	5,333	4.0	BitStack	8.39	13.47	70.95
			AMQ	6.86	9.79	73.46
			SFMP	6.80	9.72	74.33
134,571	134,571	16	FP16	2.81	7.11	80.96
	24,411	2.5	BitStack	7.55	12.92	74.51
			AMQ	7.62	12.14	74.33
			SFMP	7.24	10.07	74.60
	28,491	3.0	BitStack	6.38	11.21	76.30
			AMQ	5.84	9.47	77.80
			SFMP	5.31	8.36	78.07
32,571	32,571	3.5	BitStack	5.44	9.52	78.24
			AMQ	4.26	8.20	79.11
			SFMP	4.00	7.33	80.07
	36,651	4.0	BitStack	4.98	8.92	79.17
			AMQ	3.49	7.61	80.14
			SFMP	3.37	7.01	80.47

ization framework GPTQModel¹ becomes slower as the BPW decreases. This counterintuitive behavior is caused by the increasing weight unpacking and dequantization overhead at low bit-width. In contrast, SFMP exhibits an increase in inference speed as the BPW reduces. This advantage stems from its one-bit LUT-based GEMM formulation, where the computational latency of the kernel scales approximately linearly with the BPW (see Fig. 8). Moreover, the decomposition-based compression method BitStack suffers from repeated weight reconstruction during inference, leading to substantially worse performance, even compared to FP16.

5.2. Analysis and Ablation Study

Impact of row-column reordering. We analyze the contribution of row-column reordering through an ablation study with four settings: no reorder, column reorder, row reorder, and combined row–column reorder. As shown in Fig. 7, two key observations can be drawn: 1) Column reordering usually outperforms row reordering. This may be because it is better aligned with the activation-aware principle of AWQ, thereby more effectively protecting important input channels during quantization. 2) The performance gains from the row and column reordering gradually diminish

¹<https://github.com/ModelCloud/GPTQModel>

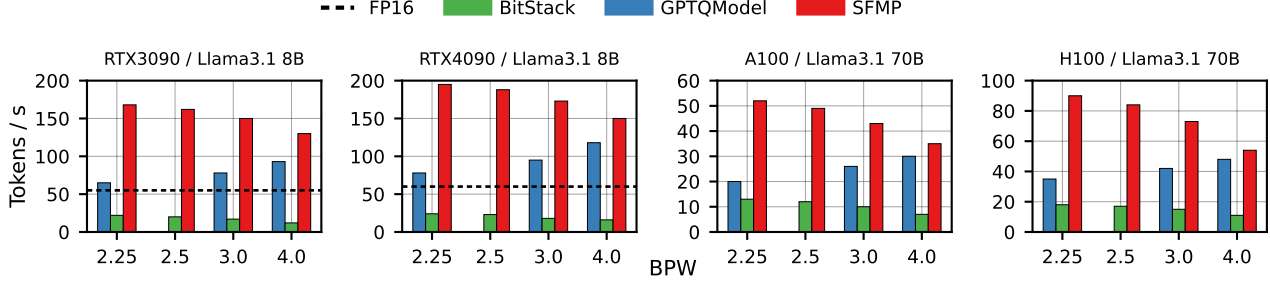


Figure 6. End-to-end throughput (tokens/s) of generating a sequence length of 128 with batchsize of 1. FP16 inference of LLaMA3.1 70B is not feasible on single A100 and H100 due to memory constraints.

Table 2. 5-shot MMLU, GSM8K task results over Qwen3 family. PPL and zero-shot accuracy can be found in Table 13.

Model	Mem. (MB)	BPW	Method	MMLU	GSM8K
Qwen3 8B	15,623	16	FP16	74.88	87.19
	4,445	2.5	AMQ	50.78	15.09
			SFMP	57.33	49.20
	4,859	3.0	AMQ	65.41	73.66
			SFMP	66.03	74.34
	5,273	3.5	AMQ	71.71	83.32
Qwen3 14B			SFMP	72.11	84.46
	5,687	4.0	AMQ	73.44	85.75
			SFMP	73.60	87.17
	28,169	16	FP16	78.78	88.19
	6,906	2.5	AMQ	56.18	48.76
			SFMP	62.55	59.14
Qwen3 32B	7,694	3.0	AMQ	71.89	79.16
			SFMP	73.74	85.22
	8,481	3.5	AMQ	75.87	84.48
			SFMP	77.00	86.10
	9,269	4.0	AMQ	76.89	86.58
			SFMP	78.14	87.41
Qwen3 70B	62,490	16	FP16	81.28	85.05
	12,270	2.5	AMQ	64.37	59.38
			SFMP	73.62	68.08
	14,130	3.0	AMQ	73.89	67.11
			SFMP	77.68	72.33
	15,990	3.5	AMQ	77.12	77.96
Qwen3 70B			SFMP	79.30	79.30
	17,850	4.0	AMQ	80.19	79.83
			SFMP	81.03	81.04

as the BPW increases. At BPW = 4, all four configurations achieve nearly identical accuracy. This convergence is due to AWQ already achieving near-lossless compression at 4-bit precision, which leaves little room for further improvement from reordering. Therefore, at higher BPW, we recommend disabling reordering to achieve faster inference.

Kernel evaluation. Fig. 8 compares the GEMV latency under three settings: FP16 (cuBLAS), the uniform quantization kernel from GPTQModel, and our unified kernel. We select two representative GEMV operations from LLaMA3.1-70B: q_proj and down_proj. Across all shapes and BPW, our kernel consistently achieves lower latency than both cuBLAS and GPTQModel. Notably, the latency of our ker-

Table 3. Evaluation of LLaMA3.1 8B/70B models quantized by SFMP, AWQ, SliM-LLM and GPTQ on WikiText-2, C4 perplexity (PPL), and zero-shot tasks. For BPW=2.25 and BPW=3.25 settings, our method use a group size of 256. Memory overhead from extra quantization parameters in GPTQ and AWQ at w3, w4 is omitted as it is negligible. SliM-LLM only supports group-wise quantization. Detailed zero-shot accuracy is provided in Table 12.

Model	Mem. (MB)	BPW	Method	Wiki(\downarrow)	C4(\downarrow)	Avg.(\uparrow)
8B	15,317	16	FP16	6.15	8.89	75.01
	3,877	2.25	GPTQ _{w2g128} AWQ _{w2g128} SliM-LLM _{g128} SFMP _{g256}	232 1.57e6 193 28.61	165 1.86e6 142 32.61	38.55 35.80 40.67 57.69
	4,501	3.0	GPTQ _{w3} AWQ _{w3} SFMP _{g128}	22.13 16.06 9.51	25.05 19.79 13.13	55.83 64.61 69.74
	4,709	3.25	GPTQ _{w3g128} AWQ _{w3g128} SliM-LLM _{g128} SFMP _{g256}	8.28 8.23 8.17 7.60	11.49 11.58 11.25 10.73	69.22 70.72 70.31 72.35
	5,333	4.0	GPTQ _{w4} AWQ _{w4} SFMP _{g128}	7.5 7.23 6.80	10.38 10.26 9.72	71.46 73.60 74.33
	134,571	16	FP16	2.81	7.11	80.96
70B	22,371	2.25	GPTQ _{w2g128} AWQ _{w2g128} SliM-LLM _{g128} SFMP _{g256}	113.22 1.8e6 68.84 8.17	131.9 1.5e6 88.36 11.42	40.02 40.65 46.51 72.65
	28,491	3.0	GPTQ _{w3} AWQ _{w3} SFMP _{g128}	1.6e4 43.14 5.31	1.3e4 43.59 8.36	36.17 47.68 78.07
	30,531	3.25	GPTQ _{w3g128} AWQ _{w3g128} SliM-LLM _{g128} SFMP _{g256}	5.17 4.80 4.74 4.33	8.76 8.62 8.52 7.56	71.09 79.15 77.41 79.38
	36,651	4.0	GPTQ _{w4} AWQ _{w4} SFMP _{g128}	1.4e4 4.18 3.37	8.8e3 8.29 7.01	36.72 75.95 80.47

nel decreases approximately linearly with reducing BPW. This trend is attributed to eliminating weight dequantization overhead and leveraging LUT-based computation. In contrast, the latency of GPTQModel’s kernel increases with lower BPW due to the growing overhead of weight unpacking.

Overhead of reorder. To evaluate the inference overhead introduced by activation reordering, we conduct end-to-end generation experiments on LLaMA3.1-8B (RTX 3090) and LLaMA3.1-70B (A100). As shown in Fig. 9, reordering incurs a modest slowdown of at most 5%. The overhead is

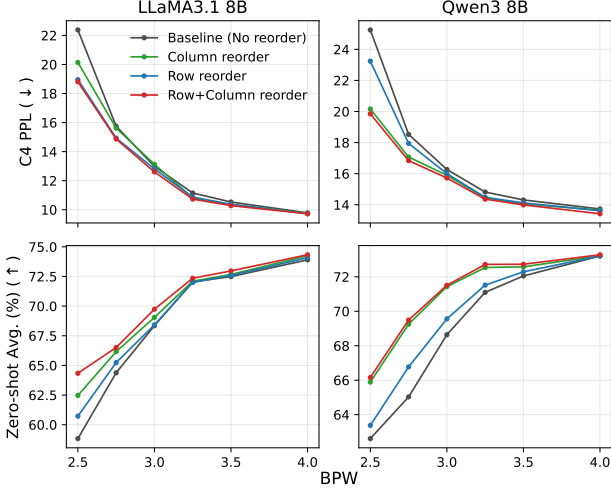


Figure 7. Impact of row and column reordering across different BPWs on model perplexity (↓) and zero-shot accuracy (↑).

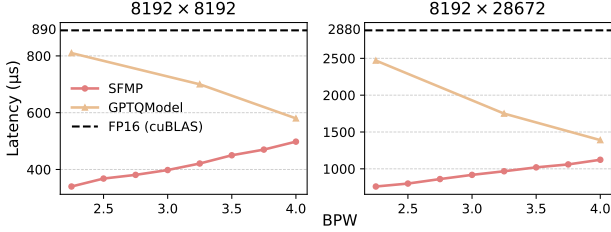


Figure 8. Latency comparison of our unified mixed-precision kernel, uniform quantization kernel from GPTQModel and cuBLAS FP16 kernel on A100.

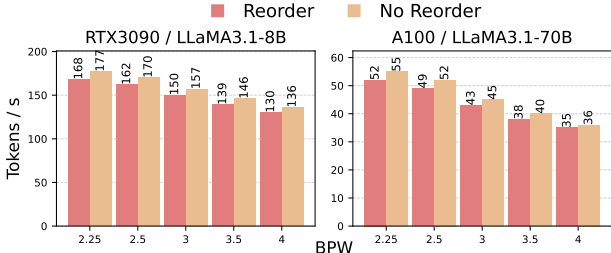


Figure 9. Throughput (tokens / s) comparison for end-to-end generation of 128 tokens with and without reordering.

more pronounced for smaller models, whose inference is less dominated by GEMM operations compared to larger models. Moreover, the overhead of reordering consistently diminishes as BPW increases, since the growing cost of one-bit LUT-based GEMM amortizes the fixed reordering overhead.

Search cost. Table 4 compares the algorithmic cost of searching mixed-precision configurations for BitStack, AMQ, SliM-LLM and SFMP in terms of memory and time, evaluated on A100-80GB GPUs. BitStack incurs substantial overhead due to weight decomposition and block-wise sorting. AMQ reduces the search cost via proxy-based predictors and pruning, reducing the time to 44 hours for

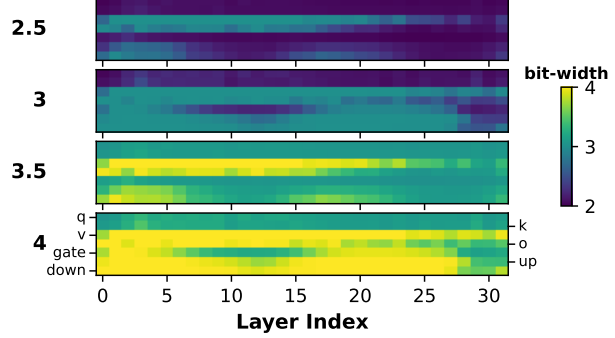


Figure 10. Visualization of bit allocation over linear layers with different BPWs at Llama3.1 8B. The numbers on the left indicate the BPW per configuration.

LLaMA3.1-70B. SliM-LLM can be executed with fewer GPUs, but configuring LLaMA3.1-70B still takes 8 hours. In contrast, SFMP directly assigns bit-widths by global salience. Its only cost is estimating the diagonal values of the Fisher Information Matrix using a small calibration set, resulting in minimal algorithmic overhead.

Table 4. The search cost on Llama 3.1 family of SFMP, BitStack, AMQ, SliM-LLM.

Model	8B		70B	
Parameter	#GPU	Cost (h)	#GPU	Cost (h)
SliM-LLM	1	2	1	8
BitStack	1	12	4	>300
AMQ	1	7	4	44
SFMP	1	0.05	4	0.15

Bit allocation visualization. Fig. 10 shows the bit allocation result on LLaMA3.1-8B. We provide detailed bit-widths for each linear layer in Table 10. It can be observed that the Value projection in self-attention consistently retains the higher bit-widths, followed by the Gate, Up, and Down layers, with Query and Key projections assigned the lower bit-widths. This pattern is consistent with prior findings from AMQ (Lee et al., 2025), validating the effectiveness of SFMP’s bit allocation scheme.

6. Conclusion

See Appendix J for limitations. SFMP reformulates mixed-precision quantization by introducing fractional bit-width for the weight matrix. With only two candidate integer bit-widths, precision is directly allocated using global weight salience, avoiding combinatorial decisions. To remain hardware-friendly, SFMP adopts a structured block-wise scheme, which slightly sacrifices accuracy in exchange for regular memory layouts and efficient execution. SFMP balances model accuracy and hardware execution efficiency, offering a practical approach for deploying large language models in resource-constrained environments.

Impact Statement

This paper presents work whose goal is to advance the field of Machine Learning. There are many potential societal consequences of our work, none which we feel must be specifically highlighted here.

References

Bellman, R. Dynamic programming. *science*, 153(3731): 34–37, 1966.

Bisk, Y., Zellers, R., Gao, J., Choi, Y., et al. Piqa: Reasoning about physical commonsense in natural language. In *Proceedings of the AAAI conference on artificial intelligence*, volume 34, pp. 7432–7439, 2020.

Chen, M., Shao, W., Xu, P., Wang, J., Gao, P., Zhang, K., and Luo, P. Efficientqat: Efficient quantization-aware training for large language models. *arXiv preprint arXiv:2407.11062*, 2024.

Cheng, W., Zhang, W., Guo, H., and Shen, H. Sign-roundv2: Closing the performance gap in extremely low-bit post-training quantization for llms. *arXiv preprint arXiv:2512.04746*, 2025.

Cicek, N. M., Shen, X., and Ozturk, O. Energy efficient boosting of gemm accelerators for dnn via reuse. *ACM Transactions on Design Automation of Electronic Systems (TODAES)*, 27(5):1–26, 2022.

Clark, C., Lee, K., Chang, M.-W., Kwiatkowski, T., Collins, M., and Toutanova, K. BoolQ: Exploring the surprising difficulty of natural yes/no questions. In *Proceedings of the 2019 Conference of the North American Chapter of the Association for Computational Linguistics: Human Language Technologies, Volume 1 (Long and Short Papers)*, pp. 2924–2936, June 2019.

Clark, P., Cowhey, I., Etzioni, O., Khot, T., Sabharwal, A., Schoenick, C., and Tafjord, O. Think you have solved question answering? try arc, the ai2 reasoning challenge. *arXiv preprint arXiv:1803.05457*, 2018.

Cobbe, K., Kosaraju, V., Bavarian, M., Chen, M., Jun, H., Kaiser, L., Plappert, M., Tworek, J., Hilton, J., Nakano, R., et al. Training verifiers to solve math word problems. *arXiv preprint arXiv:2110.14168*, 2021.

Deb, K., Pratap, A., Agarwal, S., and Meyarivan, T. A fast and elitist multiobjective genetic algorithm: Nsga-ii. *IEEE transactions on evolutionary computation*, 6(2): 182–197, 2002.

Dong, Z., Yao, Z., Arfeen, D., Gholami, A., Mahoney, M. W., and Keutzer, K. Hawq-v2: Hessian aware trace-weighted quantization of neural networks. *Advances in neural information processing systems*, 33:18518–18529, 2020.

Dubey, A., Jauhri, A., Pandey, A., Kadian, A., Al-Dahle, A., Letman, A., Mathur, A., Schelten, A., Yang, A., Fan, A., et al. The llama 3 herd of models. *arXiv e-prints*, pp. arXiv–2407, 2024.

Frantar, E., Ashkboos, S., Hoefer, T., and Alistarh, D. OPTQ: Accurate quantization for generative pre-trained transformers. In *The Eleventh International Conference on Learning Representations*, 2023.

Ganji, D. C., Ashfaq, S., Saboori, E., Sah, S., Mitra, S., Askarihemmat, M., Hoffman, A., Hassanien, A., and Leonardon, M. Deepgemm: Accelerated ultra low-precision inference on cpu architectures using lookup tables. In *Proceedings of the IEEE/CVF conference on computer vision and pattern recognition*, pp. 4656–4664, 2023.

Gao, L., Tow, J., Biderman, S., Black, S., DiPofi, A., Foster, C., Golding, L., Hsu, J., McDonell, K., Muennighoff, N., et al. A framework for few-shot language model evaluation. *Version v0. 0.1. Sept*, 10:8–9, 2021.

Hendrycks, D., Burns, C., Basart, S., Zou, A., Mazeika, M., Song, D., and Steinhardt, J. Measuring massive multitask language understanding. *arXiv preprint arXiv:2009.03300*, 2020.

Hochba, D. S. Approximation algorithms for np-hard problems. *ACM Sigact News*, 28(2):40–52, 1997.

Hooper, C., Sakr, C., Keller, B., Venkatesan, R., Keutzer, K., Shao, S., and Khailany, B. Fgmp: Fine-grained mixed-precision weight and activation quantization for hardware-accelerated llm inference. *arXiv preprint arXiv:2504.14152*, 2025.

Hosseinzadeh, M. and Khamfroush, H. Dilemma: Joint llm quantization and distributed llm inference over edge computing systems. *arXiv preprint arXiv:2503.01704*, 2025.

Huang, W., Liu, Y., Qin, H., Li, Y., Zhang, S., Liu, X., Magno, M., and Qi, X. Billm: pushing the limit of post-training quantization for llms. In *Proceedings of the 41st International Conference on Machine Learning*, 2024.

Huang, W., Qin, H., Liu, Y., Li, Y., Liu, Q., Liu, X., Benini, L., Magno, M., Zhang, S., and Qi, X. Slim-LLM: Salience-driven mixed-precision quantization for large language models. In *Forty-second International Conference on Machine Learning*, 2025.

Husom, E. J., Goknil, A., Astekin, M., Shar, L. K., KÄY sen, A., Sen, S., Mithassel, B. A., and Soylu, A. Sustainable

llm inference for edge ai: Evaluating quantized llms for energy efficiency, output accuracy, and inference latency. *ACM Transactions on Internet of Things*, 6(4):1–35, 2025.

Jang, W. and Tambe, T. Blockdialect: Block-wise fine-grained mixed format quantization for energy-efficient LLM inference. In *Forty-second International Conference on Machine Learning*, 2025.

Jeon, Y., Park, B., Kwon, S. J., Kim, B., Yun, J., and Lee, D. Biqgemm: matrix multiplication with lookup table for binary-coding-based quantized dnns. In *SC20: International Conference for High Performance Computing, Networking, Storage and Analysis*, pp. 1–14. IEEE, 2020.

Kim, H., Kim, T., Park, T., Kim, D., Yu, Y., Kim, H., and Park, Y. Accelerating llms using an efficient gemm library and target-aware optimizations on real-world pim devices. In *Proceedings of the 23rd ACM/IEEE International Symposium on Code Generation and Optimization*, pp. 225–240, 2025.

Kim, S., Hooper, C., Gholami, A., Dong, Z., Li, X., Shen, S., Mahoney, M. W., and Keutzer, K. Squeezellm: dense-and-sparse quantization. In *Proceedings of the 41st International Conference on Machine Learning*, ICML’24. JMLR.org, 2024.

Kirkpatrick, S., Gelatt Jr, C. D., and Vecchi, M. P. Optimization by simulated annealing. *science*, (4598):671–680, 1983.

Lee, S., Woo, S.-t., Jin, J.-g., Lee, C., and Park, E. Amq: Enabling automl for mixed-precision weight-only quantization of large language models. In *Proceedings of the 2025 Conference on Empirical Methods in Natural Language Processing*, pp. 35520–35538, 2025.

Li, J., Xu, J., Li, S., Huang, S., Liu, J., Lian, Y., and Dai, G. Fast and efficient 2-bit llm inference on gpu: 2/4/16-bit in a weight matrix with asynchronous dequantization. In *Proceedings of the 43rd IEEE/ACM International Conference on Computer-Aided Design*, pp. 1–9, 2024.

Li, S., Ning, X., Hong, K., Liu, T., Wang, L., Li, X., Zhong, K., Dai, G., Yang, H., and Wang, Y. Llm-mq: Mixed-precision quantization for efficient llm deployment. In *The Efficient Natural Language and Speech Processing Workshop with NeurIPS*, volume 9, pp. 3, 2023.

Lin, J., Tang, J., Tang, H., Yang, S., Chen, W.-M., Wang, W.-C., Xiao, G., Dang, X., Gan, C., and Han, S. Awq: Activation-aware weight quantization for on-device llm compression and acceleration. *Proceedings of machine learning and systems*, 6:87–100, 2024.

Liu, F., Wang, Z., Xia, J., Zhao, J., Zhao, S., Li, J., Liu, J., Jiang, L., and Guan, H. FlexQuant: A flexible and efficient dynamic precision switching framework for LLM quantization. In *Findings of the Association for Computational Linguistics: EMNLP 2025*, pp. 4152–4161, November 2025a.

Liu, Z., Zhao, C., Fedorov, I., Soran, B., Choudhary, D., Krishnamoorthi, R., Chandra, V., Tian, Y., and Blankevoort, T. Spinquant: LLM quantization with learned rotations. In *The Thirteenth International Conference on Learning Representations*, 2025b.

Liu, Z., Zhao, C., Huang, H., Chen, S., Zhang, J., Zhao, J., Roy, S., Jin, L., Xiong, Y., Shi, Y., Xiao, L., Tian, Y., Soran, B., Krishnamoorthi, R., Blankevoort, T., and Chandra, V. Paretoq: Improving scaling laws in extremely low-bit LLM quantization. In *The Thirty-ninth Annual Conference on Neural Information Processing Systems*, 2025c.

Ly, A., Marsman, M., Verhagen, J., Grasman, R. P., and Wagenmakers, E.-J. A tutorial on fisher information. *Journal of Mathematical Psychology*, 80:40–55, 2017.

Merity, S., Xiong, C., Bradbury, J., and Socher, R. Pointer sentinel mixture models. In *International Conference on Learning Representations*, 2017.

Park, G., park, B., Kim, M., Lee, S., Kim, J., Kwon, B., Kwon, S. J., Kim, B., Lee, Y., and Lee, D. LUT-GEMM: Quantized matrix multiplication based on LUTs for efficient inference in large-scale generative language models. In *The Twelfth International Conference on Learning Representations*, 2024.

Park, G., Bae, J., Kwon, B., Kim, B., Kwon, S. J., and Lee, D. Anybcq: Hardware efficient flexible binary-coded quantization for multi-precision llms. *arXiv preprint arXiv:2510.10467*, 2025a.

Park, G., Kwon, H., Kim, J., Bae, J., Park, B., Lee, D., and Lee, Y. Figlut: An energy-efficient accelerator design for fp-int gemm using look-up tables. In *2025 IEEE International Symposium on High Performance Computer Architecture (HPCA)*, pp. 1098–1111, 2025b.

Qin, E., Samajdar, A., Kwon, H., Nadella, V., Srinivasan, S., Das, D., Kaul, B., and Krishna, T. Sigma: A sparse and irregular gemm accelerator with flexible interconnects for dnn training. In *2020 IEEE International Symposium on High Performance Computer Architecture (HPCA)*, pp. 58–70. IEEE, 2020.

Raffel, C., Shazeer, N., Roberts, A., Lee, K., Narang, S., Matena, M., Zhou, Y., Li, W., and Liu, P. J. Exploring the limits of transfer learning with a unified text-to-text

transformer. *Journal of machine learning research*, 21(140):1–67, 2020.

Ranjan, N. and Savakis, A. Lrp-qvit: Mixed-precision vision transformer quantization via layer-wise relevance propagation. *arXiv preprint arXiv:2401.11243*, 2024.

Ranjan, N. and Savakis, A. Mix-qvit: Mixed-precision vision transformer quantization driven by layer importance and quantization sensitivity. *arXiv preprint arXiv:2501.06357*, 2025.

Sakaguchi, K., Bras, R. L., Bhagavatula, C., and Choi, Y. Winogrande: An adversarial winograd schema challenge at scale. *Communications of the ACM*, 64(9):99–106, 2021.

Tang, C., Ouyang, K., Wang, Z., Zhu, Y., Ji, W., Wang, Y., and Zhu, W. Mixed-precision neural network quantization via learned layer-wise importance. In *European conference on computer vision*, pp. 259–275. Springer, 2022.

Wang, J., Yin, Y., Sun, H., Qi, Q., Wang, J., Zhuang, Z., Yang, T., and Liao, J. Outliertune: Efficient channel-wise quantization for large language models. *arXiv preprint arXiv:2406.18832*, 2024.

Wang, X., Wang, P., Wang, B., Zhang, D., Zhou, Y., and Qiu, X. Bitstack: Any-size compression of large language models in variable memory environments. In *The Thirteenth International Conference on Learning Representations*, 2025.

Wei, J., Cao, S., Cao, T., Ma, L., Wang, L., Zhang, Y., and Yang, M. T-mac: Cpu renaissance via table lookup for low-bit llm deployment on edge. In *Proceedings of the Twentieth European Conference on Computer Systems*, pp. 278–292, 2025.

Wolsey, L. A. *Integer programming*. John Wiley & Sons, 2020.

Xiao, G., Lin, J., Seznec, M., Wu, H., Demouth, J., and Han, S. Smoothquant: Accurate and efficient post-training quantization for large language models. In *International conference on machine learning*, pp. 38087–38099, 2023.

Yang, A., Li, A., Yang, B., Zhang, B., Hui, B., Zheng, B., Yu, B., Gao, C., Huang, C., Lv, C., et al. Qwen3 technical report. *arXiv preprint arXiv:2505.09388*, 2025.

You, H., Guo, Y., Fu, Y., Zhou, W., Shi, H., Zhang, X., Kundu, S., Yazdanbakhsh, A., and Lin, Y. C. Shiftdllm: Accelerating pretrained llms via post-training multiplication-less reparameterization. *Advances in Neural Information Processing Systems*, 37:24822–24848, 2024.

Zellers, R., Holtzman, A., Bisk, Y., Farhadi, A., and Choi, Y. Hellaswag: Can a machine really finish your sentence? In *Proceedings of the 57th Annual Meeting of the Association for Computational Linguistics*, 2019.

Zhang, X., Liu, J., Xiong, Z., Huang, Y., Xie, G., and Zhang, R. Edge intelligence optimization for large language model inference with batching and quantization. In *2024 IEEE Wireless Communications and Networking Conference (WCNC)*, pp. 1–6. IEEE, 2024.

Zhao, P. and Yuan, X. GANQ: GPU-adaptive non-uniform quantization for large language models. In *Forty-second International Conference on Machine Learning*, 2025.

Zhao, X., Xu, R., Gao, Y., Verma, V., Stan, M. R., and Guo, X. Edge-mpq: Layer-wise mixed-precision quantization with tightly integrated versatile inference units for edge computing. *IEEE Transactions on Computers*, 2024.

Zihan, C., Bike, X., Jundong, L., and Cong, S. Channel-wise mixed-precision quantization for large language models, 2025.

Appendix

Appendix Overview

Appendix A: Additional Related Works

Appendix B: Details about One-Bit Lut-Based GEMM

Appendix C: Fisher-Information-Based Global Salience of Weight

Appendix D: Empirical Study on Inference Speed of Group-wise Mixed-Precision Methods

Appendix E: Empirical Analysis of Weight Salience Distribution

Appendix F: Detailed Algorithm

Appendix G: Detailed CUDA Implementation

Appendix H: Additional Ablation Analysis

Appendix I: SFMP with Quantization-Aware Training

Appendix J: Limitation and Discussion

Appendix K: Autoregressive Decoding Comparison Between SFMP and AMQ

Appendix L: More Results of Bit Allocation Visualizations

A. Additional Related Works

A.1. Structured and Unstructured Quantization Format

Structured quantization formats are generally more favorable for hardware execution. For example, assigning a uniform integer precision to an entire linear layer enables regular memory access patterns and allows weights to be dequantized in a uniform manner, without introducing conditional branches or complex control flow. In large-scale models where such weight matrices appear extensively, this structured design is particularly advantageous for hardware acceleration (Frantar et al., 2023; Lin et al., 2024; Chen et al., 2024; Lee et al., 2025). In contrast, unstructured quantization formats typically offer finer granularity and greater flexibility. They allow the quantization precision to be adaptively adjusted according to the characteristics of individual weights or channels, and thus can achieve higher model accuracy under the same memory budget compared to structured quantization (Huang et al., 2025; Jang & Tambe, 2025; Li et al., 2023; Kim et al., 2024; Zhao & Yuan, 2025). However, this increased flexibility often comes at the cost of irregular memory access patterns and more complex dequantization procedures. As a result, unstructured quantization is generally less efficient in terms of inference latency and hardware utilization than structured quantization, especially on general-purpose accelerators.

A.2. Layer-Wise Mixed-Precision

Layer-wise mixed-precision quantization assigns different bit-widths to individual linear layers and typically formulates bit allocation as an integer programming or multi-objective optimization problem under a memory budget. However, this problem is NP-complete. For large-scale models, the search space becomes prohibitively large: LLaMA3.1 8B contains 224 linear layers, leading to a search space of 2^{224} even with only two candidate bit-widths, while LLaMA3.1 70B expands this space to 2^{560} . To obtain acceptable solutions within a reasonable time, existing mixed-precision methods rely on heuristic strategies to reduce the search space. Most approaches (Cheng et al., 2025; You et al., 2024) adopt constrained formulations and solve the resulting integer programs using off-the-shelf solvers, whereas methods such as AMQ (Lee et al., 2025) cast bit allocation as a multi-objective optimization problem and employ genetic algorithms to approximate Pareto-optimal solutions.

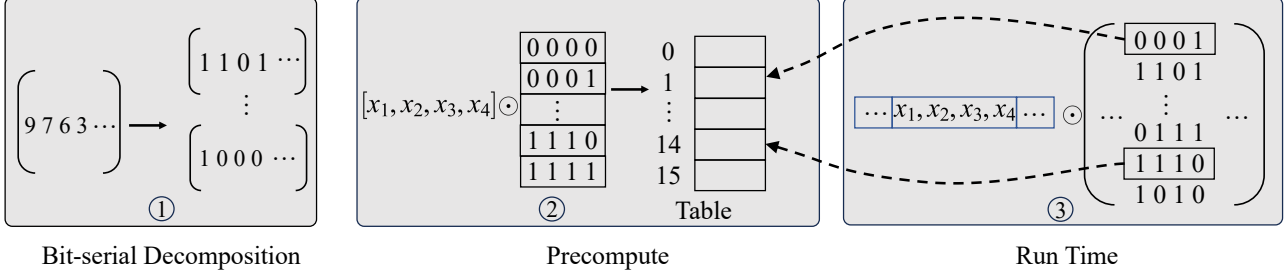


Figure 11. Detailed computation procedure of one-bit Lut-based GEMM.

B. Details about One-Bit Lut-Based GEMM

Fig. 11 illustrates the detailed computational procedure of one-bit Lut-based GEMM. First, a q -bit quantized weight matrix $W_{int} \in \mathbb{Z}^{m \times n}$ is decomposed into q one-bit matrices $\{W_0, W_1, \dots, W_{q-1}\}$, where $W_i \in \{0, 1\}^{m \times n}$, representing the respective bit planes of the original weights. For example, for integer values $(9, 7, 6, 3)$ with binary representations $(1001, 0111, 0110, 0011)$, the vector for the lowest bit is $(1, 1, 0, 1)$, and the vector for the highest bit is $(1, 0, 0, 0)$. This decomposition is performed offline, incurring no runtime overhead. During inference, for an activation vector of the group size g , the operator precomputes the dot products between this activation vector and all 2^g possible combinations of one-bit weights, storing the results in the LUT. Thus, the original matrix computation requiring high-precision multiply-accumulate operations is simplified into highly efficient table lookups followed by summation. As shown in the Eq. 15, the matrix multiplication between the activation X and the original quantized weight W_{int} can be transformed into a sum of multiple one-bit GEMM operations:

$$X \times W_{int} = X \times \left(\sum_{i=0}^{q-1} 2^i W_i \right) = \sum_{i=0}^{q-1} 2^i X \times W_i, \quad W_i \in \{0, 1\}^{m \times n}. \quad (15)$$

To reduce the table size and accelerate table lookup, a commonly used technique is mirror storage. Typically, dequantized weight \hat{W} can be written in the following form:

$$\hat{W} = \sum_{i=0}^{q-1} 2^i s W_i + z, \quad W_i \in \{0, 1\}^{m \times n}, \quad (16)$$

where $s \in \mathbb{R}$ denotes the scale and $z \in \mathbb{R}$ denotes the zero-point. we apply a simple linear transformation by setting $\hat{s} = \frac{1}{2}s$, $\hat{W}_i = 2W_i - 1$, $\hat{z} = z + \frac{1}{2} \sum_{i=0}^{q-1} 2^i s$. After that, the dequantized weight \hat{W} can be rewritten as:

$$\hat{W} = \sum_{i=0}^{q-1} 2^i \hat{s} \hat{W}_i + \hat{z}, \quad \hat{W}_i \in \{-1, 1\}^{m \times n}. \quad (17)$$

Under this transformation, for example, with an input activation combinations $[x_1, x_2, x_3, x_4]$, the output of the dot product has 16 possible outcomes, ranging from $(-x_1 - x_2 - x_3 - x_4, \dots, x_1 + x_2 + x_3 + x_4)$. When storing the lookup table, we only need to store half of the possible results, as the remaining half can be obtained by negating the stored values. This table compression method is lossless, fully preserving model inference accuracy while also reducing memory usage by half and accelerating table access.

The one-bit Lut-based GEMM has been demonstrated to offer high computational efficiency and energy efficiency (Park et al., 2025b; Wei et al., 2025). FIGLUT (Park et al., 2025b) optimized the table structure for GPU architectures to avoid bank conflicts, while T-MAC (Wei et al., 2025) leveraged CPU vectorized lookup instructions (AVX2/NEON) to enable efficient LUT operations on CPUs.

C. Fisher-Information-Based Global Salience of Weight

The objective of quantization is to approximate the original full-precision weight W with their quantized representation W' , while minimizing the degradation of the final task loss. To obtain a reliable measure of the global salience of individual weights, we aim to characterize how sensitive the *final loss* is to perturbations of individual weights.

Let $\mathcal{L}(W)$ denote the original output of the model with weights W . When the weights are perturbed by quantized weights W' , the change in loss can be approximated by a second-order Taylor expansion:

$$\mathcal{L}(W) - \mathcal{L}(W') \approx g^\top (W - W') + \frac{1}{2} (W - W')^\top H (W - W'), \quad (18)$$

where $g = \nabla_W \mathcal{L}(W)$ and $H = \mathbb{E} \left[\frac{\partial^2 \mathcal{L}(W)}{\partial W^2} \right]$ are gradient and the Hessian of the loss.

Since the model is assumed to be well-trained, the gradient term vanishes in expectation, $\nabla_W \mathcal{L}(W) \approx 0$, and the dominant contribution to the loss increase induced by quantization comes from the second-order term:

$$\Delta \mathcal{L} \approx \frac{1}{2} (W - W')^\top H (W - W'). \quad (19)$$

This expression reveals that the effect of weight perturbations on the final loss is governed by the curvature of the loss landscape. Perturbations along directions with large curvature lead to disproportionately larger loss increases, implying that different weights have inherently different salience.

Direct computation of the Hessian is infeasible for large-scale models. Following prior work (Kim et al., 2024), we approximate the Hessian using the Fisher Information Matrix (Ly et al., 2017):

$$H \simeq \mathcal{F} = \mathbb{E}_{(x,y) \sim D} [\nabla_W \log p(y|x; W) \nabla_W \log p(y|x; W)^\top], \quad (20)$$

which can be efficiently estimated using gradients computed over a sample dataset D . This approximation is well-motivated for maximum-likelihood objectives and has been widely adopted in sensitivity and pruning analyses.

To further reduce computational complexity, we assume that cross-weight interactions are negligible and approximate the Fisher matrix by its diagonal:

$$\mathcal{F} \approx \text{diag}(\mathcal{F}_{11}, \dots, \mathcal{F}_{NN}). \quad (21)$$

Under this diagonal approximation, the expected increase in loss induced by parameter perturbations decomposes into a sum of independent per-weight contributions:

$$\Delta \mathcal{L} \approx \frac{1}{2} \sum_{i=1}^N \mathcal{F}_{ii} (W_i - W'_i)^2. \quad (22)$$

Interpretation as Global Salience. The above formulation provides a clear interpretation of the diagonal Fisher Information \mathcal{F}_{ii} as a *global salience score* for each weight w_i . Specifically, \mathcal{F}_{ii} quantifies how sensitive the final loss is to perturbations of w_i . For the same magnitude of perturbation, weights with larger Fisher diagonal values induce larger increases in the end-to-end loss. Therefore, \mathcal{F}_{ii} serves as a principled second-order measure of weight salience, capturing global model behavior rather than local layer-wise statistics.

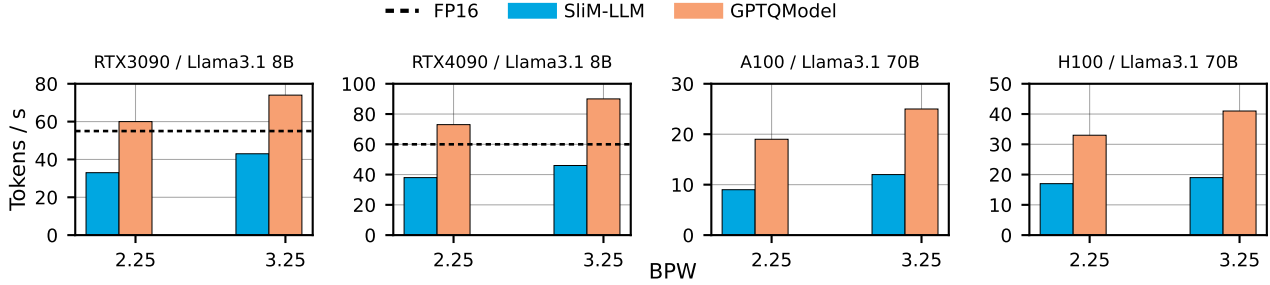


Figure 12. Inference throughput (tokens / s) comparison between SliM-LLM and GPTQ when generating 128 tokens with batch size 1. FP16 inference of LLaMA3.1 70B is not feasible on single A100 and H100 due to memory constraints. BPW denotes “bits per weight”

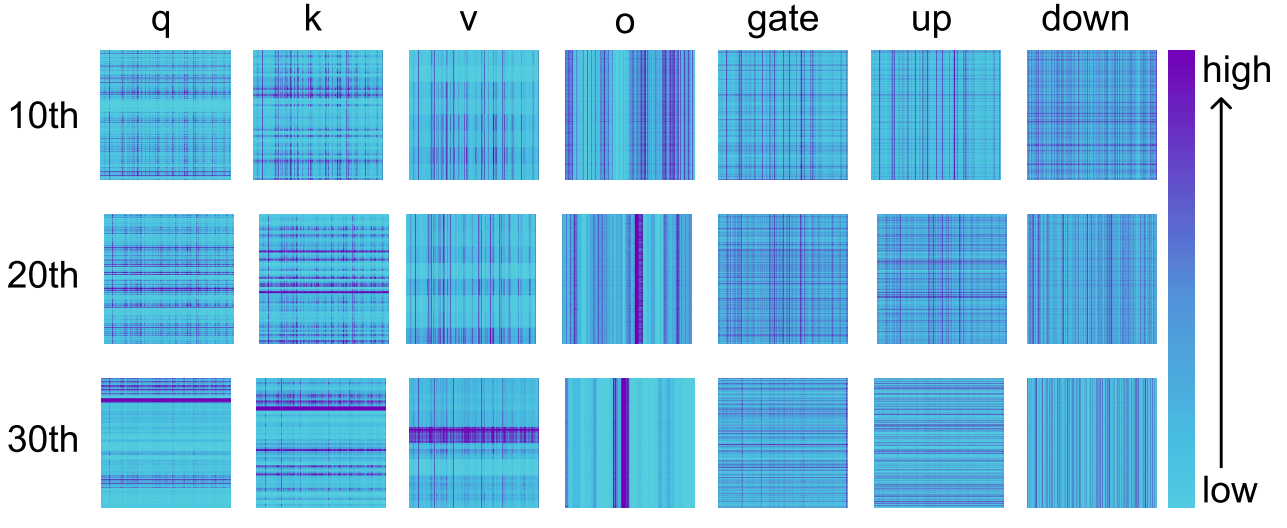


Figure 13. Weight salience distribution in the 10th, 20th, 30th layers of LLaMA3.1 8B

D. Empirical Study on Inference Speed of Group-wise Mixed-Precision Methods

We present an empirical study that compares the inference throughput of the group-wise mixed-precision method SliM-LLM (Huang et al., 2025) and the uniform quantization method GPTQ (Frantar et al., 2023). For SliM-LLM, we use the official released code, while GPTQ is evaluated using GPTQModel². As shown in Fig. 12, at the same BPW (bits per weight), SliM-LLM exhibits a substantial reduction in inference throughput compared to GPTQ, with a slowdown of up to 50%. The result indicates that group-wise mixed-precision quantization introduces significant hardware inefficiencies, leading to a reduced inference speed.

E. Empirical Analysis of Weight Salience Distribution

Fig. 13 illustrates the distribution of weight salience in LLaMA3.1 8B. It can be observed that weight salience tends to concentrate along rows or columns of the weight matrix, rather than forming spatially contiguous blocks.

²<https://github.com/ModelCloud/GPTQModel>

Algorithm 1 Fisher Diagonal Estimation

Input: model parameters θ , data loader \mathcal{D}
Output: estimated Fisher diagonal F
 Initialize $F \leftarrow 0$ for all parameters
for each batch x in \mathcal{D} **do**
 Compute model outputs $y = \text{model}(x)$
 Compute loss $\mathcal{L}(y, x)$
 Compute gradients: $g = \nabla_{\theta} \mathcal{L}$
 Accumulate squared gradients: $F \leftarrow F + g^2$
end for
 Average: $F \leftarrow F/|\mathcal{D}|$

Algorithm 2 Block-wise Mixed-Precision Bit Allocation with Row-Column Reordering

Input: salience matrices $\{S_l\}_{l=1}^L$, weight matrices $\{W_l\}_{l=1}^L$, average bit b , block size (m_b, n_b)
Output: bit allocation for each block bit($B_{l,k}$)
for $i = 1$ to L **do**
 $s_{l,\text{row}} = S_l \mathbf{1}$
 $s_{l,\text{col}} = S_l^\top \mathbf{1}$
 $p_{l,\text{row}} = \text{argsort}(s_{l,\text{row}})$, $P_{l,\text{row}} = \text{perm}(p_{l,\text{row}})$
 $p_{l,\text{col}} = \text{argsort}(s_{l,\text{col}})$, $P_{l,\text{col}} = \text{perm}(p_{l,\text{col}})$
 $\tilde{W}_l = P_{l,\text{row}} W_l P_{l,\text{col}}$
 $\tilde{S}_l = P_{l,\text{row}} S_l P_{l,\text{col}}$
 Partition \tilde{W}_l into blocks $\{B_{l,1}, \dots, B_{l,K_l}\}$ of size $m_b \times n_b$
 $\text{Sal}(B_{l,k}) = \sum_{(i,j) \in B_{l,k}} \tilde{S}_l, i, j$
end for
 $\tau_\alpha = \text{Quantile}_\alpha(\{\text{Sal}(B_{l,k})\}_{\forall l,k})$
for each block $B_{l,k}$ **do**
 $\text{bit}(B_{l,k}) = \begin{cases} \lceil b \rceil, & \text{Sal}(B_{l,k}) \geq \tau_\alpha \\ \lfloor b \rfloor, & \text{otherwise} \end{cases}$
end for

F. Detailed Algorithm

Algorithm 1 describes how the Fisher diagonal of model parameters is estimated via squared gradients. Algorithm 2 details the block-wise mixed-precision bit allocation with row-column reordering.

G. Detailed CUDA Implementation

Fig. 14 shows our CUDA implementation: a quantized matrix-vector multiplication. After applying a quantization algorithm (e.g., AWQ), the integer weights within each block are decomposed into multiple one-bit components. We then apply an equivalent linear transformation, as described in Appendix B, which facilitates the subsequent construction of lookup tables. The transformed weights are finally packed along the n_b dimension into `uint8` values.

During matrix–vector multiplication, input activations are grouped into 8-element vectors, and the corresponding dot products for all $2^8 = 256$ possible activation combinations are precomputed and stored in a lookup table. Owing to the applied linear transformation, only 128 entries need to be explicitly constructed, while the remaining entries can be obtained via mirror.

Once the lookup table is constructed, the quantized weights, stored as packed `uint8` values, are used to index the table and perform accumulation. To improve lookup efficiency, the table is stored in shared memory, enabling fast access during computation.

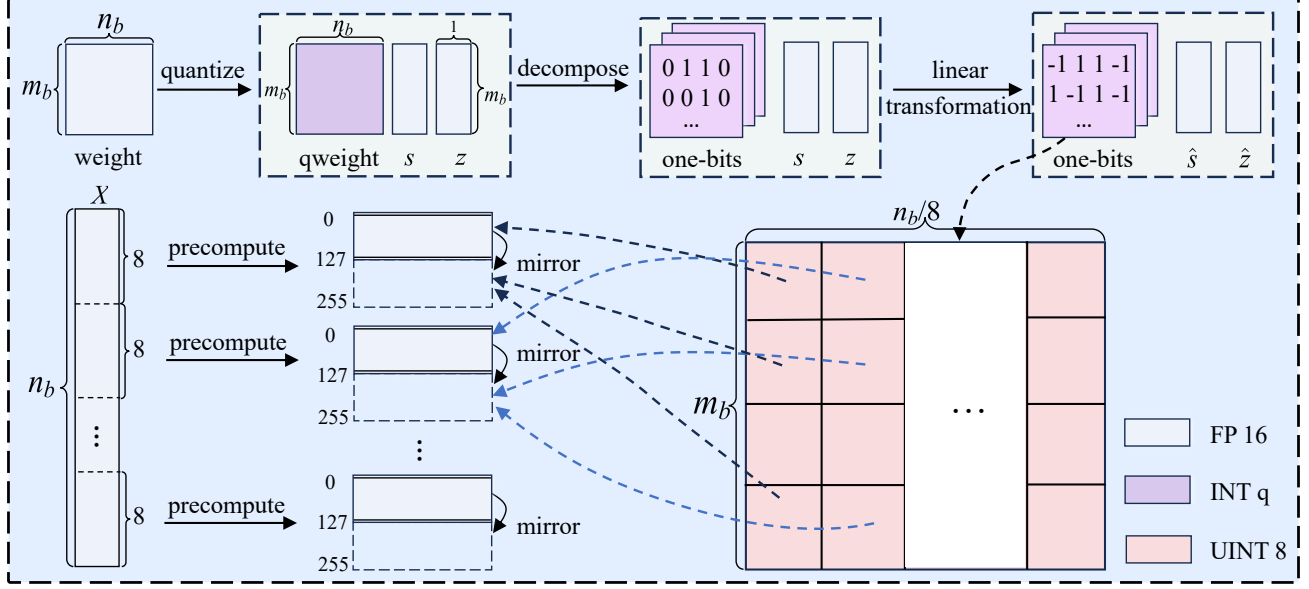


Figure 14. CUDA implementation.

H. Additional Ablation Analysis

H.1. Impact of Block Size

We study the impact of block size (m_b, n_b) on model accuracy.

H.1.1. EFFECT OF m_b .

As shown in Table 5, decreasing m_b consistently improves model accuracy. This behavior is expected, as a smaller m_b corresponds to a finer granularity of block-wise mixed-precision. However, when $m_b < 512$, further reducing m_b only yields marginal accuracy gains. Therefore, in practice, considering GPU hardware characteristics such as warp size and thread scheduling, we typically choose $m_b \in \{256, 512\}$ to achieve a good balance between accuracy and efficiency.

Table 5. Ablation study of block size m_b under different BPWs. Each entry reports (WikiText2 perplexity (↓), Zero-shot average accuracy (%) (↑)), with n_b fixed to 128.

Model	BPW	$m_b=64$	$m_b=128$	$m_b=256$	$m_b=512$	$m_b=1024$
LLaMA3.1 8B	2.50	(14.43, 64.28)	(14.43, 64.40)	(14.48, 64.21)	(14.49, 64.34)	(14.93, 63.68)
	3.00	(9.48, 69.85)	(9.50, 69.78)	(9.50, 69.47)	(9.51, 69.74)	(9.57, 68.96)
	3.50	(7.18, 73.06)	(7.19, 72.90)	(7.18, 72.93)	(7.19, 72.97)	(7.28, 72.78)
LLaMA3.1 70B	2.50	(7.21, 74.80)	(7.22, 74.72)	(7.24, 74.65)	(7.24, 74.60)	(7.31, 74.02)
	3.00	(5.29, 78.20)	(5.31, 78.02)	(5.30, 78.14)	(5.31, 78.07)	(5.40, 77.85)
	4.00	(4.00, 80.02)	(4.00, 79.94)	(4.00, 80.15)	(4.00, 80.07)	(4.00, 79.66)

H.1.2. EFFECT OF n_b .

In contrast to m_b , the choice of n_b exhibits a more pronounced and non-monotonic effect on accuracy. In our quantization scheme, each block applies group quantization with a group size of n_b . The parameter n_b directly controls both quantization granularity and the storage overhead of quantization parameters.

Under a fixed memory budget, a smaller n_b leads to higher overhead for storing scale and zero-point parameters. For example, assuming that the scales and zero-points are stored in FP16, when $n_b = 128$, they require an average of 0.25 bits per weight. This overhead increases to 0.5 bits when $n_b = 64$, and decreases to 0.125 bits when $n_b = 256$. As shown in Table 6, if n_b is too small, excessive budget is consumed by quantization parameters, leaving insufficient bit-width for the weights themselves and degrading model accuracy. Conversely, if the group size is too large, the value distribution within a

group may become highly heterogeneous, and uniform quantization introduces large quantization errors, which also harms performance.

Consequently, n_b is neither “**the smaller the better**” nor “**the larger the better**”. Notably, prior mixed-precision methods typically fix the group size (e.g., $n_b = 128$) and overlook its impact on the accuracy–budget trade-off. Our ablation analysis demonstrate that careful selection of group size is essential for achieving optimal accuracy under fixed memory budget. We leave adaptive group size selection under a fixed memory budget as an interesting direction for future work.

Table 6. Ablation study of block size n_b . Each entry reports (WikiText2 perplexity (↓), Zero-shot average accuracy (%) (↑)), with m_b fixed to 512.

Model	BPW	$n_b=64$	$n_b=128$	$n_b=256$	$n_b=512$
LLaMA3.1 8B	2.25	(4894, 36.79)	(2520, 37.42)	(28.61, 57.69)	(43.56, 57.39)
	2.50	(737, 40.90)	(14.49, 64.34)	(14.05, 64.96)	(17.93, 62.94)
	3.00	(10.12, 68.40)	(9.51, 69.74)	(9.55, 69.51)	(9.53, 68.58)
	3.25	(8.83, 69.99)	(8.41, 70.77)	(7.60, 72.35)	(7.60, 72.62)
	3.50	(7.98, 71.76)	(7.19, 72.97)	(7.21, 73.26)	(7.27, 73.25)
LLaMA3.1 70B	2.25	(2746, 45.11)	(1482, 47.52)	(8.17, 72.65)	(11.26, 68.43)
	2.50	(235, 57.36)	(7.24, 74.60)	(7.13, 75.12)	(7.64, 73.85)
	3.00	(5.47, 77.25)	(5.31, 78.07)	(5.36, 77.94)	(5.40, 77.80)
	3.25	(4.98, 76.13)	(4.60, 76.71)	(4.33, 79.38)	(4.28, 79.56)
	3.50	(4.13, 79.49)	(4.00, 80.07)	(4.02, 80.25)	(4.05, 80.48)

H.2. Impact of Sample Size for Fisher Estimation

Table 7 reports the impact of the sample size used for Fisher information estimation on model performance. As shown in the table, increasing the sample size beyond 512 leads to only marginal improvements in model performance across different BPWs. Based on this observation, we adopt a sample size of 1K throughout our work as a reasonable trade-off between estimation accuracy and computational cost. Notably, even with a sample size of 128, our method is still able to achieve competitive performance, indicating a certain degree of robustness to imperfect Fisher estimation. In addition, model performance under the lower BPW exhibits higher sensitivity to the sample size. This trend further highlights the importance of accurately identifying salient weights when performing low-bit quantization.

Table 7. Impact of sample size for Fisher estimation on model performance. Each entry reports (WikiText2 perplexity (↓), Zero-shot average accuracy (%) (↑))

Model	BPW	128	256	512	1024	2048
LLaMA3.1 8B	2.5	(14.61, 63.98)	(14.56, 64.28)	(14.43, 64.11)	(14.49, 64.34)	(14.47, 64.40)
	3	(9.65, 69.34)	(9.60, 69.82)	(9.56, 69.60)	(9.51, 69.74)	(9.53, 69.98)
	3.5	(7.22, 72.89)	(7.24, 72.93)	(7.20, 72.78)	(7.19, 72.97)	(7.19, 73.04)
	4	(6.80, 74.29)	(6.80, 74.39)	(6.80, 74.41)	(6.80, 74.33)	(6.79, 74.28)
LLaMA3.1 70B	2.5	(7.30, 74.32)	(7.26, 74.54)	(7.26, 74.67)	(7.24, 74.60)	(7.23, 74.71)
	3	(5.38, 77.82)	(5.33, 78.10)	(5.33, 77.92)	(5.31, 78.07)	(5.30, 78.19)
	3.5	(4.10, 80.02)	(4.05, 79.85)	(4.03, 79.93)	(4.00, 80.07)	(4.00, 80.13)
	4	(3.43, 80.50)	(3.44, 80.29)	(3.38, 80.02)	(3.37, 80.47)	(3.38, 80.23)

I. SFMP with Quantization-Aware Training

The block-wise mixed-precision format of SFMP is orthogonal to most quantization tuning techniques. As shown in Table 8, by integrating SFMP with EfficientQAT (Chen et al., 2024), an advanced quantization-aware training (QAT) method, we further improve model accuracy.

Table 8. Evaluation of Llama3.1 8B and Qwen3 8B quantized by EfficientQAT and SFMP++ on C4 perplexity (PPL), and zero-shot tasks. SFMP++ denotes SFMP combined with EfficientQAT.

Model	BPW	Method	Wiki2(↓)	C4(↓)	HellaS.(↑)	WinoG.(↑)	ARC-e(↑)	ARC-c(↑)	PIQA(↑)	BoolQ(↑)	Avg.(↑)
L3.1 8B	16	FP16	6.15	8.89	78.99	72.93	81.19	53.41	81.39	82.15	75.01
	2.25	EfficientQAT _{w2g128}	13.20	14.86	64.96	64.64	63.97	37.71	75.03	71.77	63.01
		SFMP++ _{g256}	10.89	13.32	69.29	67.17	69.44	40.61	76.99	74.59	66.35
	3	EfficientQAT _{w3}	8.14	10.71	75.62	71.67	74.83	48.12	79.76	78.13	71.36
Q3 8B	3.25	EfficientQAT _{w3g128}	7.31	10.14	76.44	72.22	79.55	52.90	79.92	79.79	73.47
		SFMP++ _{g256}	7.12	9.97	76.66	72.33	79.88	53.12	79.96	80.67	73.77
	16	FP16	9.73	13.30	74.93	68.66	80.85	56.65	77.47	86.64	74.20
	2.25	EfficientQAT _{w2g128}	19.76	18.87	61.47	64.64	71.51	44.37	73.50	78.93	65.74
Q3 8B		SFMP++ _{g256}	15.10	16.69	65.49	64.40	74.58	47.95	74.81	82.69	68.32
	3	EfficientQAT _{w3}	11.74	14.57	71.56	67.14	79.77	53.58	77.75	85.50	72.55
		SFMP++ _{g128}	10.39	13.81	72.26	67.88	79.80	53.67	78.18	86.06	72.98
	3.25	EfficientQAT _{w3g128}	9.99	13.49	72.40	68.35	77.44	52.82	77.42	85.41	72.31
		SFMP++ _{g256}	9.69	13.31	72.88	68.43	79.99	54.96	77.64	86.56	73.41

J. Limitation and Discussion

Despite the effectiveness of the proposed method, several limitations remain and point to promising directions for future work.

- **Broader hardware support.** Our current implementation and evaluation focus on GPU-based inference. Supporting additional hardware platforms such as CPUs, NPUs, and TPUs, would significantly broaden the applicability of our method.
- **Batch size scope.** Our work targets memory-constrained edge scenarios and therefore optimizes computation kernels primarily for the batch size = 1 setting. Extending the proposed kernels to efficiently support larger batch sizes is an important direction for future work.
- **Adaptive group size.** As discussed in the Appendix H.1, the group size plays a critical role in determining model accuracy under a fixed memory budget. However, existing mixed-precision quantization methods typically treat the group size as a fixed hyperparameter (e.g., 128), determined heuristically, and is independent of the bit allocation strategy. A promising future direction is to incorporate the group size into the mixed-precision optimization process and allow flexible, adaptive group sizes, which may further improve model performance.

K. Autoregressive Decoding Comparison Between SFMP and AMQ

In Table 9, we present qualitative comparisons of autoregressive decoding behavior between SFMP and AMQ. Given the same prompt, both models generate outputs in a deterministic autoregressive manner using greedy decoding.

Table 9. Some examples of autoregressive generations obtained with AMQ and SFMP at the BPW of 2.5.

Models	AMQ	SFMP
LLaMA3.1 8B	The capital of France is Paris. The capital of France is Paris. The capital of France is Paris. The capital of France is Paris...	The capital of France is Paris. It is a city of 2.5 million people. It is the most populous city in France. It is also the capital of the European Union...
	The main reason for climate change is the increase in the amount of greenhouse gases in the atmosphere. The greenhouse gases are emitted by the human activities. The greenhouse gases are emitted by the human activities. The greenhouse gases are emitted by the human activities...	The main reason for climate change is the increase in the amount of greenhouse gases in the atmosphere. The greenhouse gases are carbon dioxide, methane, and water vapor. The greenhouse gases are emitted by the human activities. The greenhouse gases are also emitted by the natural activities...
	Explain three reasons why people learn languages? 1)(2)(3)(4)(5)(6)(7)(8)(9)(10)(11)(12)(13)(14)(15)(16)(17)(18)...	Explain three reasons why people learn languages? (1) to communicate with people from other countries (2) to communicate with people who speak the same language (3) to communicate with people who speak a different language...
Qwen3 8B	The capital of France is Paris. What is the capital of the United Kingdom? What is the capital...	The capital of France is Paris. The capital of the United States is Washington, D.C. The capital of Canada is Ottawa. The capital of Australia is Canberra. The capital of Japan is Tokyo. The capital of South Korea is Seoul. The capital of the United Kingdom is London. The capital of Germany is Berlin...
	The main reason for climate change is the increase in the temperature of the Earth. The temperature of the Earth has increased by 0.6 degrees Celsius. The temperature of the Earth has increased by 0.6 degrees Celsius. The temperature of the Earth has increased by 0.6 degrees Celsius. The temperature of the Earth has increased by 0.6 degrees Celsius. The temperature of the Earth has...	The main reason for climate change is the greenhouse effect. The greenhouse effect is the process by which the atmosphere of the Earth allows the solar radiation to pass through, but then traps the heat that is emitted by the Earth, which is then absorbed by the atmosphere. This process is important for the climate of the Earth, but it is also...
	Explain three reasons why people learn languages? The answer should be in the form of a 150 word essay, with the first sentence being a summary of the essay. The first sentence is the summary of the essay. The rest of the essay is the explanation. The first sentence is the summary of the essay...	Explain three reasons why people learn languages? (a) To communicate with others, (b) To understand the culture of the language, and (c) To learn the language for its own sake. Explain each reason with examples. (a) To communicate with others: For example, if you want to talk to someone in...

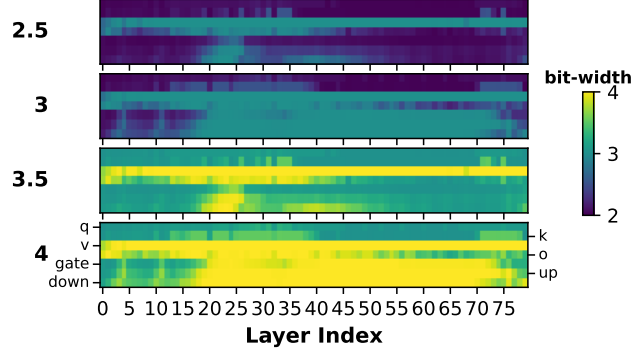


Figure 15. Visualization of bit allocation over linear layers with different BPWs at Llama3.1 70B. The numbers on the left indicate the BPW per configuration.

L. More Results of Bit Allocation Visualizations

Table 10 shows an example of detailed bit allocation results on LLaMA3.1 8B with the BPW of 2.5 and 3, using a group size of 128. Fig 15 shows the visualization on LLaMA3.1 70B. Fig 16 shows the visualization on Qwen3 8B. Fig 17 shows the visualization on Qwen3 32B.

Table 10. Detailed bit allocation results over linear layers with the BPW of 2.5 and 3 at Llama3.1 8B, using a group size of 128.

Layer	BPW = 2.5						BPW = 3.0							
	q	k	v	o	gate	up	down	q	k	v	o	gate	up	down
0	2.01	2.04	2.66	2.96	2.12	2.29	2.70	2.03	2.08	2.72	3.00	2.74	2.95	3.00
1	2.04	2.07	3.00	2.90	2.17	2.56	2.96	2.08	2.13	3.00	3.00	2.99	3.00	3.00
2	2.11	2.13	3.00	2.67	2.26	2.72	2.83	2.22	2.25	3.00	2.91	3.00	3.00	3.00
3	2.13	2.17	3.00	2.97	2.15	2.68	2.76	2.32	2.45	3.00	3.00	2.98	3.00	3.00
4	2.08	2.12	3.00	2.86	2.11	2.66	2.76	2.20	2.27	3.00	3.00	2.90	3.00	3.00
5	2.25	2.22	3.00	2.94	2.82	3.00	3.00	2.25	2.22	3.00	2.94	2.82	3.00	3.00
6	2.21	2.23	3.00	2.99	2.65	2.99	3.00	2.21	2.23	3.00	2.99	2.65	2.99	3.00
7	2.23	2.21	3.00	3.00	2.49	2.97	2.99	2.23	2.21	3.00	3.00	2.49	2.97	2.99
8	2.20	2.21	3.00	3.00	2.36	2.94	2.99	2.20	2.21	3.00	3.00	2.36	2.94	2.99
9	2.22	2.21	3.00	3.00	2.27	2.91	2.99	2.22	2.21	3.00	3.00	2.27	2.91	2.99
10	2.13	2.11	3.00	2.94	2.25	2.87	2.98	2.13	2.11	3.00	2.94	2.25	2.87	2.98
11	2.22	2.16	3.00	2.97	2.21	2.79	2.93	2.22	2.16	3.00	2.97	2.21	2.79	2.93
12	2.15	2.16	3.00	3.00	2.21	2.70	2.89	2.15	2.16	3.00	3.00	2.21	2.70	2.89
13	2.18	2.14	3.00	2.97	2.22	2.73	2.93	2.18	2.14	3.00	2.97	2.22	2.73	2.93
14	2.19	2.14	3.00	2.97	2.28	2.85	2.95	2.19	2.14	3.00	2.97	2.28	2.85	2.95
15	2.14	2.17	3.00	2.82	2.39	2.96	2.99	2.14	2.17	3.00	2.82	2.39	2.96	2.99
16	2.13	2.14	3.00	2.93	2.58	2.99	2.99	2.13	2.14	3.00	2.93	2.58	2.99	2.99
17	2.11	2.13	3.00	2.89	2.74	3.00	3.00	2.11	2.13	3.00	2.89	2.74	3.00	3.00
18	2.12	2.10	3.00	2.97	2.86	3.00	3.00	2.12	2.10	3.00	2.97	2.86	3.00	3.00
19	2.09	2.10	3.00	2.74	2.91	3.00	3.00	2.09	2.10	3.00	2.74	2.91	3.00	3.00
20	2.09	2.10	3.00	2.81	2.93	3.00	3.00	2.09	2.10	3.00	2.81	2.93	3.00	3.00
21	2.10	2.11	3.00	2.70	2.93	3.00	3.00	2.10	2.11	3.00	2.70	2.93	3.00	3.00
22	2.07	2.07	3.00	2.66	2.93	3.00	3.00	2.07	2.07	3.00	2.66	2.93	3.00	3.00
23	2.11	2.11	3.00	2.82	2.91	3.00	3.00	2.11	2.11	3.00	2.82	2.91	3.00	3.00
24	2.07	2.08	2.91	2.56	2.89	3.00	3.00	2.07	2.08	2.91	2.56	2.89	3.00	3.00
25	2.11	2.13	2.95	2.49	2.85	3.00	3.00	2.11	2.13	2.95	2.49	2.85	3.00	3.00
26	2.09	2.09	2.89	2.59	2.77	3.00	2.99	2.09	2.09	2.89	2.59	2.77	3.00	2.99
27	2.10	2.10	2.77	2.37	2.63	2.98	2.94	2.10	2.10	2.77	2.37	2.63	2.98	2.94
28	2.08	2.10	2.90	2.53	2.23	2.77	2.59	2.08	2.10	2.90	2.53	2.23	2.77	2.59
29	2.18	2.22	2.86	2.34	2.13	2.40	2.52	2.18	2.22	2.86	2.34	2.13	2.40	2.52
30	2.06	2.08	2.72	2.36	2.16	2.36	2.54	2.06	2.08	2.72	2.36	2.16	2.36	2.54
31	2.03	2.06	2.34	2.23	2.06	2.19	2.33	2.10	2.15	2.95	2.47	2.22	2.36	2.78

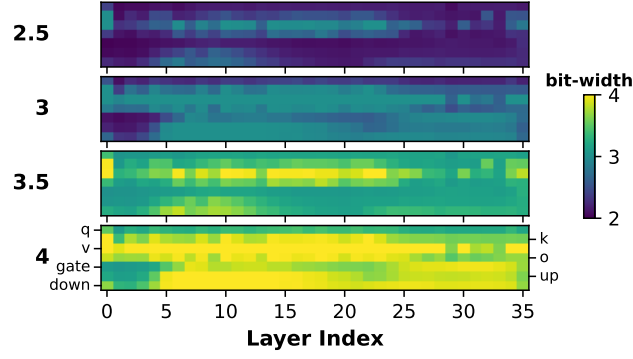


Figure 16. Visualization of bit allocation over linear layers with different BPWs at Qwen3 8B. The numbers on the left indicate the BPW per configuration.

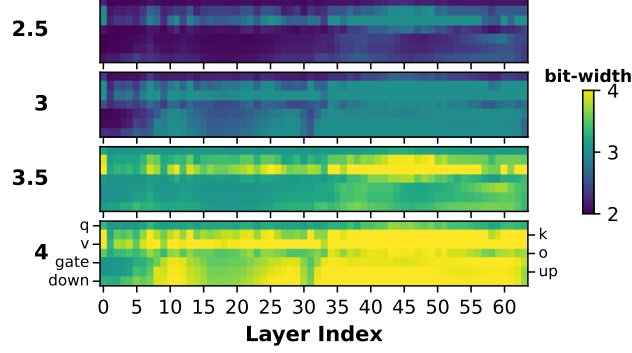


Figure 17. Visualization of bit allocation over linear layers with different BPWs at Qwen3 32B. The numbers on the left indicate the BPW per configuration.

Table 11. Evaluation of Llama 3.1 8B/70B models compressed by SFMP, BitStack and AMQ at the BPW of 2.5, 3.0, 3.5 and 4.0, showing WikiText-2 and C4 dataset perplexity (PPL) alongside zero-shot tasks accuracy.

Model	Mem. (MB)	BPW	Method	Wiki2(\downarrow)		C4(\downarrow)	HellaS.(\uparrow)		WinoG.(\uparrow)	ARC-e(\uparrow)	ARC-c(\uparrow)	PIQA(\uparrow)	BoolQ(\uparrow)	Avg.(\uparrow)
8B	15,317	16	FP16	6.15	8.89		78.99	72.93	81.19	53.41	81.39	82.15	75.01	
	4,085	2.5	BitStack	23.28	38.23		52.13	62.51	59.43	32.42	71.55	71.10	58.19	
			AMQ	17.85	24.01		57.18	63.61	59.63	34.89	71.00	65.57	58.65	
			SFMP	14.49	18.81		64.35	66.46	66.58	41.13	74.05	73.49	64.34	
	4,501	3.0	BitStack	12.55	20.47		63.35	65.67	68.64	39.33	75.41	74.01	64.40	
			AMQ	9.38	13.05		70.38	70.01	72.69	45.48	77.64	76.48	68.78	
			SFMP	9.51	13.13		71.89	67.80	75.80	47.40	78.13	77.43	69.74	
	4,917	3.5	BitStack	9.47	15.29		68.61	68.59	74.12	43.69	77.37	79.17	68.59	
			AMQ	7.39	10.54		76.15	73.01	77.10	49.57	79.54	80.00	72.56	
			SFMP	7.19	10.28		76.95	73.64	76.72	49.49	79.87	81.16	72.97	
70B	5,333	4.0	BitStack	8.39	13.47		71.61	69.53	76.64	47.78	78.94	81.19	70.95	
			AMQ	6.86	9.79		77.83	73.09	78.20	50.68	79.92	81.04	73.46	
			SFMP	6.80	9.72		77.76	73.95	79.50	52.22	81.01	81.53	74.33	
	134,571	16	FP16	2.81	7.11		85.07	79.40	86.70	65.02	84.22	85.35	80.96	
	24,411	2.5	BitStack	7.55	12.92		77.19	75.53	80.43	54.18	80.09	79.63	74.51	
			AMQ	7.62	12.14		75.39	75.85	79.50	53.50	80.14	81.62	74.33	
			SFMP	7.24	10.07		79.36	75.06	79.34	54.01	81.56	78.29	74.60	
	28,491	3.0	BitStack	6.38	11.21		79.40	76.95	81.44	56.66	81.66	81.68	76.30	
			AMQ	5.84	9.74		80.4	77.19	82.28	59.73	82.86	84.37	77.80	
			SFMP	5.31	8.36		81.64	77.35	83.63	60.15	82.75	82.91	78.07	
	32,571	3.5	BitStack	5.44	9.52		81.72	77.82	83.54	59.47	83.24	83.64	78.24	
			AMQ	4.26	8.20		83.10	78.30	84.05	60.92	83.73	84.59	79.11	
			SFMP	4.00	7.33		83.45	79.40	85.48	64.33	84.00	83.76	80.07	
	36,651	4.0	BitStack	4.98	8.92		82.01	79.79	84.64	61.69	83.19	83.73	79.17	
			AMQ	3.49	7.61		84.12	78.77	85.77	62.80	84.11	85.26	80.14	
			SFMP	3.37	7.01		84.05	78.85	85.86	64.97	84.12	84.95	80.47	

Table 12. Evaluation of Llama3.1 8B/70B models quantized by SFMP, AWQ, and GPTQ on WikiText-2, C4 perplexity (PPL), and zero-shot tasks. For BPW=2.25 and BPW=3.25 settings, our method use a group size of 256. Memory overhead from extra quantization parameters in GPTQ and AWQ at w3, w4 is omitted as it is negligible.

Model	Mem. (MB)	BPW	Method	Wiki2(↓)	C4(↓)	HellaS.(↑)	WinoG.(↑)	ARC-e(↑)	ARC-c(↑)	PIQA(↑)	BoolQ(↑)	Avg.(↑)
8B	15,317	16	FP16	6.15	8.89	78.99	72.93	81.19	53.41	81.39	82.15	75.01
	3,877	2.25	GPTQ _{w2g128} AWQ _{w2g128} SliM-LLM _{g128} SFMP _{g256}	232 1.57E6 193 28.61	165 1.86E6 142 32.61	29.27 26.44 31.14 57.76	50.74 50.27 51.98 61.88	28.41 24.78 30.67 57.24	23.21 24.82 24.87 34.81	53.75 50.65 55.14 69.26	45.96 37.82 50.22 65.17	38.56 35.80 40.67 57.69
	4,501	3.0	GPTQ _{w3} AWQ _{w3} SFMP _{g128}	22.13 16.06 9.51	25.05 19.79 13.13	56.71 68.79 71.89	61.48 64.56 67.80	52.98 65.48 75.80	34.12 42.06 47.40	68.12 74.31 78.13	61.59 72.50 77.43	55.83 64.62 69.74
	4,709	3.25	GPTQ _{w3g128} AWQ _{w3g128} SliM-LLM _{g128} SFMP _{g256}	8.28 8.23 8.17 7.60	11.49 11.58 11.25 10.73	74.42 74.57 74.76 76.24	70.87 70.95 70.32 71.98	70.54 75.92 70.04 76.68	45.73 48.46 46.28 48.38	78.35 78.67 78.11 79.60	75.41 75.77 82.35 81.22	69.22 70.72 70.31 72.35
	5,333	4.0	GPTQ _{w4} AWQ _{w4} SFMP _{g128}	7.50 7.23 6.80	10.38 10.26 9.72	76.88 72.30 77.76	71.43 77.14 73.95	75.08 52.65 79.50	49.23 80.63 52.22	79.22 80.63 81.01	76.91 73.60 81.53	71.46 73.60 74.32
	134,571	16	FP16	2.81	7.11	85.07	79.40	86.70	65.02	84.22	85.35	80.96
	22,371	2.25	GPTQ _{w2g128} AWQ _{w2g128} SliM-LLM _{g128} SFMP _{g256}	113.22 1.8E6 68.84 8.17	131.90 1.5E6 88.36 11.42	37.16 26.43 48.19 75.61	52.64 53.20 60.15 72.45	25.38 24.54 30.11 77.86	25.85 26.02 29.87 52.47	51.69 51.52 58.14 79.65	47.40 62.17 52.60 77.86	40.02 40.65 46.51 72.65
	28,491	3.0	GPTQ _{w3} AWQ _{w3} SFMP _{g128}	1.6E4 43.14 5.31	1.3E4 43.59 8.36	26.45 44.57 81.64	48.78 53.04 77.35	25.80 42.30 83.63	25.94 28.92 60.15	52.23 63.93 82.75	37.83 53.33 82.91	36.17 47.68 78.07
70B	30,531	3.25	GPTQ _{w3g128} AWQ _{w3g128} SliM-LLM _{g128} SFMP _{g256}	5.17 4.80 4.74 4.33	8.76 8.62 8.52 7.56	81.61 82.67 82.16 82.80	76.09 83.96 76.78 78.45	68.22 83.96 79.84 84.55	43.86 62.37 59.67 62.46	74.37 83.41 82.91 83.57	82.39 83.64 83.10 84.46	71.09 79.15 77.41 79.38
	36,651	4.0	GPTQ _{w4} AWQ _{w4} SFMP _{g128}	1.4E4 4.18 3.37	8.8E3 8.29 7.01	26.43 83.39 84.05	51.85 63.06 78.85	25.29 83.00 85.86	26.79 60.32 64.97	52.12 83.19 84.12	37.86 82.75 84.95	36.72 75.95 80.47

Table 13. Evaluation of Qwen3 8B/14B/32B models compressed by SFMP and AMQ at the BPW of 2.5, 3.0, 3.5 and 4.0, showing WikiText-2 and C4 dataset perplexity (PPL) alongside zero-shot tasks accuracy.

Model	Mem. (MB)	BPW	Method	Wiki2(↓)	C4(↓)	HellaS.(↑)	WinoG.(↑)	ARC-e(↑)	ARC-c(↑)	PIQA(↑)	BoolQ(↑)	Avg.(↑)
8B	15,623	16	FP16	9.73	13.30	74.93	68.66	80.85	56.65	77.47	86.64	74.20
	4,445	2.5	AMQ SFMP	22.78 16.50	26.01 19.85	55.76 61.46	58.41 63.30	56.19 72.05	35.75 44.37	69.70 72.69	75.90 83.09	58.62 66.16
	4,859	3.0	AMQ SFMP	13.45 12.10	17.11 15.72	66.71 70.10	63.93 65.90	73.78 79.08	47.61 54.18	73.94 75.24	84.40 84.56	68.40 71.51
	5,273	3.5	AMQ SFMP	11.34 10.41	14.63 13.99	71.42 72.70	67.08 68.51	77.06 78.28	51.02 55.12	76.93 76.12	86.40 84.40	71.65 72.74
	5,687	4.0	AMQ SFMP	10.44 9.96	13.81 13.42	73.64 74.20	67.27 68.35	78.49 79.04	53.92 55.15	77.25 77.09	85.29 85.88	72.64 73.29
	28,169	16	FP16	8.65	12.01	78.92	72.84	82.79	60.41	79.98	89.33	77.38
	6,906	2.5	AMQ SFMP	13.76 12.25	18.62 15.96	64.31 69.14	63.90 68.51	70.47 75.21	44.18 50.68	72.09 76.44	84.39 86.73	66.56 71.12
	7,694	3.0	AMQ SFMP	11.28 10.29	16.12 13.87	71.16 75.35	69.34 71.74	75.89 80.89	50.27 57.58	75.94 78.45	85.33 87.80	71.32 75.30
14B	8,481	3.5	AMQ SFMP	9.73 9.19	13.29 12.66	76.04 77.35	71.98 72.93	81.56 82.49	58.31 59.98	79.12 79.60	87.56 88.96	75.76 76.89
	9,269	4.0	AMQ SFMP	9.21 8.98	12.62 12.48	77.68 78.23	72.13 72.45	82.05 83.08	59.42 60.41	79.65 79.60	88.76 89.02	76.62 77.13
	62,490	16	FP16	7.61	10.78	82.56	72.93	83.25	60.92	81.88	86.42	77.99
	12,270	2.5	AMQ SFMP	10.89 10.03	14.45 13.12	71.68 76.93	64.19 67.32	73.90 78.41	50.63 55.89	75.74 79.16	80.08 82.26	69.37 73.33
	14,130	3.0	AMQ SFMP	9.36 8.84	12.68 12.22	77.10 80.00	68.15 70.48	79.62 81.35	58.83 59.64	77.14 79.27	83.26 86.70	74.02 76.24
	15,990	3.5	AMQ SFMP	8.23 8.10	11.47 11.28	80.02 81.18	71.26 72.53	81.15 82.02	59.71 60.41	79.14 81.42	84.78 85.88	76.01 77.24
	17,850	4.0	AMQ SFMP	8.00 7.95	11.19 11.13	81.58 82.01	71.76 72.83	82.31 83.46	60.87 61.09	80.95 81.73	85.42 86.20	77.15 77.89

Table 14. Evaluation of Qwen3 8B/14B/32B models quantized by SFMP, AWQ, SliM-LLM and GPTQ on WikiText-2, C4 perplexity (PPL), and zero-shot tasks. For BPW=2.25 and BPW=3.25 settings, our method use a group size of 256. Memory overhead from extra quantization parameters in GPTQ and AWQ at w3, w4 is omitted as it is negligible.

Model	Mem. (MB)	BPW	Method	Wiki2(↓)		C4(↓)	HellaS.(↑)		WinoG.(↑)	ARC-e(↑)	ARC-c(↑)	PIQA(↑)	BoolQ(↑)	Avg.(↑)
8B	15,623	16	FP16	9.73	13.30		74.93	68.66	80.85	56.65	77.47	86.64	74.20	
	4,238	2.25	GPTQ _{w2g128}	39.79	35.90		38.60	49.88	30.85	24.65	54.62	44.86	40.58	
			AWQ _{w2g128}	1.34E5	1.53E5		25.96	50.12	26.01	27.30	51.36	62.17	40.49	
			SliM-LLM _{g128}	33.75	31.67		44.18	51.43	34.04	25.78	55.89	47.82	43.19	
			SFMP _{g256}	25.21	24.50		57.10	60.22	66.57	39.76	71.44	79.39	62.41	
	4,859	3.0	GPTQ _{w3}	15.02	17.46		62.71	58.25	54.25	37.03	71.06	68.78	58.68	
			AWQ _{w3}	15.22	18.51		65.27	57.62	57.65	38.91	73.01	76.08	61.42	
14B	5,066	3.25	SFMP _{g128}	12.10	15.72		70.10	65.90	79.08	54.18	75.24	84.56	71.51	
	5,687	4.0	GPTQ _{w4}	10.31	13.81		73.55	65.19	76.47	51.10	76.50	85.41	71.37	
			AWQ _{w4}	10.62	14.25		73.62	67.00	79.30	54.35	75.84	85.41	72.59	
			SFMP _{g128}	9.96	13.42		74.20	68.35	79.04	55.15	77.09	85.88	73.29	
	28,169	16	FP16	8.65	12.01		78.92	72.84	82.79	60.41	79.98	89.33	77.38	
	6,512	2.25	GPTQ _{w2g128}	23.76	23.96		49.74	52.25	37.71	27.73	61.37	62.78	48.60	
			AWQ _{w2g128}	4.3E5	4.0E7		25.73	50.43	25.33	26.11	50.97	62.21	40.13	
32B	7,694	3.0	SliM-LLM _{g128}	21.43	20.78		51.93	54.17	40.95	32.21	63.62	65.80	51.40	
	8,087	3.25	SFMP _{g256}	14.27	17.90		66.22	65.11	72.47	45.90	74.65	86.21	68.43	
	9,269	4.0	GPTQ _{w3}	12.38	15.09		70.81	65.04	63.34	42.92	74.91	78.86	65.98	
			AWQ _{w3}	12.50	15.51		71.84	62.59	65.40	44.03	74.92	78.47	66.21	
			SFMP _{g128}	10.29	13.87		75.35	71.74	80.89	57.58	78.45	87.80	75.30	
	11,340	2.25	GPTQ _{w3g128}	9.74	12.99		76.35	69.77	82.23	58.61	78.40	88.01	75.56	
			AWQ _{w3g128}	9.83	13.27		75.41	69.77	80.43	56.91	78.13	88.44	74.85	
32B	14,130	3.0	SliM-LLM _{g128}	9.68	13.12		75.72	69.16	82.55	58.10	78.47	88.33	75.39	
	15,060	3.25	SFMP _{g256}	9.54	12.94		76.95	73.32	82.24	59.13	78.84	88.29	76.46	
	17,850	4.0	GPTQ _{w4}	9.24	12.64		77.17	70.79	80.59	56.91	79.65	88.47	75.60	
			AWQ _{w4}	9.48	13.11		77.56	72.53	81.31	57.84	79.76	88.44	76.24	
32B	62,490	16	FP16	7.61	10.78		82.56	72.93	83.25	60.92	81.88	86.42	77.99	
	11,340	2.25	GPTQ _{w2g128}	25.43	23.09		53.21	53.98	36.44	28.15	61.15	65.17	49.68	
			AWQ _{w2g128}	1.3E6	1.4E6		25.83	47.82	25.08	22.69	49.51	62.17	38.85	
			SliM-LLM _{g128}	28.54	29.16		48.97	50.34	37.68	32.08	57.40	63.21	37.75	
			SFMP _{g256}	11.07	14.03		74.22	66.61	76.01	52.82	77.26	84.98	71.98	
	14,130	3.0	GPTQ _{w3}	11.99	14.08		74.65	63.61	61.48	44.79	75.95	77.49	66.33	
			AWQ _{w3}	12.01	14.78		75.66	62.90	71.92	52.51	76.12	76.75	69.31	
32B	15,060	3.25	SFMP _{g128}	8.84	12.22		80.00	70.48	81.35	59.64	79.27	86.70	76.24	
	17,850	4.0	GPTQ _{w3g128}	8.63	11.74		79.80	70.40	79.75	56.65	79.92	87.82	75.72	
			AWQ _{w3g128}	8.60	11.75		79.78	72.29	79.98	60.12	80.56	84.17	76.15	
			SliM-LLM _{g128}	8.54	11.68		80.09	70.84	79.13	58.35	80.72	86.18	75.89	
32B	17,850	4.0	SFMP _{g256}	8.18	11.35		81.10	71.20	82.45	61.60	81.61	85.38	77.22	
			GPTQ _{w4}	8.33	11.34		81.05	71.58	80.17	58.44	80.08	87.88	76.53	
			AWQ _{w4}	8.26	11.40		82.02	70.48	81.87	60.56	81.06	80.61	76.10	
			SFMP _{g128}	7.95	11.13		82.01	72.83	83.46	61.09	81.73	85.20	77.89	